Contents list available at CBIORE journal website

International Journal of Renewable Energy Development

Journal homepage: https://ijred.cbiore.id

Research Article

# Solar adsorption cooling system operating by activated–carbon–ethanol bed

Mena Safaa Mohammed and Nibal Fadel Farman Alhialy*

*Department of Energy, Engineering College, University of Baghdad, Iraq*

**Abstract**. One efficient way to convert small thermally energized into effective cooling is through adsorption cooling technology, which increases energy efficiency and reduces environmental pollution. This study's primary goal is to hypothetically examine the thermal coefficient of performing the solar adsorptive refrigerator machine operated with an activating carbon/Ethanol operating dual. The impact of different operating situations and design factors on the machine's performance is inspected and evaluated. The present double-bed solar energy adsorptive-cooler unit is modeled by thermodynamic methodology. Then, it was analyzed to evaluate its effectiveness work under Baghdad climate conditions. For the current study, the two-bed solar adsorption cooling unit with 0.5 kW capacity input heat 11893 that operates at 5 °C for the evaporator and 45 °C for the condenser is presented. The Engineering-Equation-Solver (EES) simulation program was created and used to solve the modeling equations that predict the optimal cycle performance and evaluate the optimum reasonable values of the operation parameters of the proposed system. The pressure range for the refrigeration cycle is 2.408 kPa for the evaporation state and 23.14 kPa for the condensation state. The findings demonstrate that an optimum coefficient of performance (COP) is 0.702 at 95 °C, a 20% performance increase, which generates 39.4 of cooling water. It produced 1 kg of chilled water for 2.463 kg of activated carbon at a temperature of 5°C. The improved solar-powered adsorption systems and refrigeration technologies are appealing substitutes that can satisfy energy demands in addition to meeting needs for cooling, ice production, air conditioning, and refrigeration preservation and safeguarding of the environment with Iraq's climate conditions.

**Keywords:** solar refrigerator, adsorption, equilibrium uptake, cooling, specific cooling power, performance.

@ The author(s). Published by CBIORE. This is an open-access article under the CC BY-SA license (http://creativecommons.org/licenses/by-sa/4.0/).

Received: 9th February 2024; Revised: 20th March 2024; Accepted: 28th March 2024; Available online: 2d April 2024

## 1. Introduction

The confluence of shifting climate dynamics alongside the evolution of human civilization has precipitated a surging demand for cooling infrastructure. Refrigeration, a pivotal domain, holds an insignificant role in fostering the progress and sustainability global economy, contributing substantially to diverse spheres of human life, encompassing aspects like food preservation, pharmaceutical storage, and ensuring thermal comfort. Nonetheless, the refrigeration sector remains a notable provider of greenhouse gas emissions (GHG), accounting for 7.8% of the total emissions. Traditional refrigeration systems utilize refrigerants characterized by an escalating concentration of greenhouse gases, thereby contributing to circumstances conducive to extraordinary global warming (GWP) and depletion of the ozone layer. These refrigerants notably include Chloro-fluoro-carbons (CFCs), hydro-chlorofluoro-carbons (HCFCs), and hydro-fluoro-carbons (HFCs), collectively responsible for 37% of emissions. The remaining 63% release steam indirectly from the consumption energy associated with refrigeration and air conditioning systems (Khanam *et al.,* 2018)

The imperative to sustain renewable energy contributions worldwide, driven by the objective to mitigate greenhouse gas emissions, has piqued the interest of nations. This has catalyzed research endeavors focused on exploring sustainable alternatives for cooling systems. The harnessing of renewable energy sources, notably solar power derived from natural reservoirs such as sunlight stands as a logical proposition, particularly in regions like Iraq endowed with abundant solar energy resources. In Iraq, the scarcity of electricity contrasts sharply with the abundant solar irradiation, underscoring the paramount significance of leveraging solar energy to ameliorate the sweltering conditions prevalent in the region. Iraq's climatic conditions present a compelling case for harnessing solar energy, displaying an immensely favorable potential. Moreover, research has included solar modules that are specially designed to match the climate of Iraq, providing appropriate options for sustainable energy applications (Ahmed & Farman Alhialy, 2019, Ahmed & Alhialy, 2020 and Saadoon *et al.*, 2020).

Iraq boasts an impressive richness of solar energy radiation, averaging between 1,800-2,390, kilowatt-hours per square meter per year of direct normal irradiation. Spearheading advancements in solar technology would not only signify a resurgence in the country's technical capabilities but also foster the development of Iraqi expertise in a promising field, potentially leading to significant export opportunities (Patrick & Khalidah, n.d. and Abass & Pavlyuchenko, 2019).

The goal of this research is to introduce and implement solar energy utilization within Iraq as a renewable energy source specifically toward facilitating cooling processes, especially during the summer. The utilization of adsorption refrigeration systems for cooling production presents a promising and

* Corresponding author
Email: dr.nibal.f@coeng.uobaghdad.edu.iq (N.F.F. Alhialy)

https://doi.org/10.61435/ijred.2024.60170
ISSN: 2252-4940/© 2024.The Author(s). Published by CBIORE

sustainable solution applicable across various sectors. These systems can be directly powered by small-grading thermal energy sources, establishing a viable option. Reducing dependence on refrigerants with high global warming aligns with sustainability objectives

## 2. Literature Review

Two essential components of existence are cooling and water. Adsorption cooling and desalination systems applications environmentally friendly refrigerants like water, methanol, ethanol, ammonia, $CO_2$, and organic hydrocarbons, offering a compelling avenue toward sustainable cooling solutions. Adsorption systems were classified as open (for dehumidification and air conditioning) or closed (for freezing, cooling, and air conditioning) (Elsheniti *et al*., 2018; Boruta *et al.,* 2021**;** Saha *et al.,* 2016; Mustafa *et a*l, 2024 and Gautam *et al.,* 2024).

Broadly, adsorbent and adsorbate working pairs in adsorption cooling systems can be categorized into three types—physical, chemical, and composite adsorbents—based on the forces involved in the adsorption process. Physical working pairs (PWP) rely on van der Waals forces to capture and retain the adsorbate. Examples of physical working pairs include zeolite with water (Sowunmi *et al.,* 2023) by utilizing the TRNSYS 16.0 simulation software, model, assess the viability of refrigeration from a system that employs a combination of zeolite-based adsorbents and water ($H_2O$) as adsorbate pairs via four solar concentrating collectors, two for adsorption and two for desorption.

Patel & Maiti, (2023) reported that the solar adsorption-cooling machine with zeolite13X-water as an adsorbent-adsorbate pair was designed, fabricated, and experimentally investigated. Rupa *et al.* (2020) experimentally investigated activated carbon-graphene composite/ethanol pairs as working pairs for solar adsorption systems. The tested data equilibrium of uptake was fitted with the D-A (Dubinin- Astakhov) equation.

In addition, silica gel with water, metal-organic frameworks (MOFs) with water and ethanol (Chen *et al*., 2019), activated carbon with methanol, ethanol, or ammonia, activated carbon fiber with methanol, alcohol, or ammonia, and composite materials involving polymers as working pair. The characterization of physical working pairs can be achieved through two specific methods: the volumetric method and the gravimetric method. These methodologies help measure and evaluate the effectiveness and performance of physical working pairs in adsorption cooling systems (Tarish *et al*., 2020)

Ethanol, (ethyl alcohol or $C_2H_5OH$), due to its low point of freezing, is recounted as a dependable refrigerant. Chemically stable, non-toxicity, zero-ozone-depletion, and minimal potential for global warming. Ethanol with activated carbon combined, has been thoroughly investigated as a potential working fluid. However, the adsorption heat associated with ethanol is relatively lower compared to methanol, typically lying within the range of 1000 to 900 kJ/kg. Ethanol possesses eco-friendly attributes and is non-toxic, distinct from methanol. Besides, ethanol exhibits a reasonably higher evaporation pressure even at lower levels of temperature, rendering it a superior and sustainable alternative as a working fluid (Tarish *et al.,* 2020**)**.

The investigations and studies dealing with solar adsorption refrigeration systems cover experimental applications, theoretical investigation, simulation, modeling, and connecting the two sectors. In the context of ice formation inside solar adsorption refrigeration systems, the results showed that activated carbon combined with methanol performed better than activated carbon paired with ethanol. This discrepancy in performance points to different behaviors and efficiency of the adsorption-desorption processes between the two working pairs, which affects how well the system can create ice (Li *et al.,* 2004).

An intermittent carbon-ethanol refrigerator has been modeled mathematically. Adsorber temperature is regulated using cooled water, while condenser temperature is controlled with hot and cold oil at predetermined temperatures. It is possible to assess the temperature in the chilled box, the amount of ethanol exiting and reabsorbed, and the temperature of the working pair in the adsorber. There is a compatible agreement between the experimental and simulated works (El-Sharkawy *et al.,* 2006 and Tiansuwan and Hirunlabh, 1998).

Insightful findings were obtained from a thorough investigation of ethanol-paired activated carbon fibers (ACF) for adsorption cooling systems (El-Sharkawy *et al.,* 2008 and 2015). Researchers looked closely at the combined adsorptive capacity ratings of A-15 and A-20 ethanol/activated carbon fiber. The equilibrium adsorption capacity of the A-20/ethanol pair was found to be substantially larger than that of the A-15/ethanol pair, according to the results. The Maxsorb III/ethanol duo has significant promise for solar cooling applications, as demonstrated by the determination of adsorption isotherms for this combination. The study found that employing this particular adsorption pair in a cooling unit might achieve an impressive COP and (SCP), as high as 0.8 and 420 kJ/kg, respectively. A heat source at 80°C and a heat sink at 30°C might be used to achieve this notable cooling effect with an evaporation temperature of 7°C. These results highlight this adsorption pair's great potential for producing significant cooling effects in solar-powered refrigeration systems.

Bouzid *et al*., (2019) investigated the ethanol adsorption isotherms using two types of phenol resin-constructed adsorbents, potassium hydroxide subjected to spherical phenol resin treatment (KOH4-PR and KOH6-PR), using statistical physical treatment. Different mass quantities of spherical phenol resin were treated to produce these adsorbents. The purpose of the study was to comprehend how ethanol adsorbed on these various sorbents at various temperature ranges. The results showed that for KOH4-PR and KOH6-PR, the ethanol adsorption concentration on the sorbents was 1.43 and two kg of ethanol/kg of adsorbent, respectively.

Chauhan *et al.,* (2024) and Abdulkadir *et al.,* (2022) prepared a new activated carbon (ACs) adsorbent with ethanol as adsorbate and date-seed activated carbon (DSAC) for use as adsorbent with methanol for the adsorption-cooling machine, by using experimental data on ethanol and methanol uptake to determine the Dubinin-Astakhov (D-A) model's structural constants accurately. The study emphasizes how ideal the suggested ACs are for effective, long-lasting heat-pumping and cooling applications with low–grade energy.

In recent times, El-Sharkawy *et al.,* (2014) conducted experimental research to describe adsorbent materials suitable for application in adsorptive refrigeration machines. Brancato *et al*., (2015) explored using a silica gel crowd matrix bed and several commercial activated carbons in combination with ethanol as a refrigerant, as well as a porosity compound that was created appropriately out of lithium bromide. Based on the experimental data, a thermodynamic evaluation of each adsorbent pair's attainable performance was determined by computing the highest possible COP (Coefficient of Performing) for air conditioning and refrigeration applications under normal operating boundary circumstances. The novel composite material has the best thermodynamic performances, 0.64-0.72, under both of the assessed working conditions.

Uddin *et al*., (2014) investigated an adsorption pair, Maxsorb 3/ethanol. The experimental characteristics of surface-treated Maxsorb 3 with controlled oxygen concentration and "parent" Maxsorb 3 with ethanol adsorption were investigated. The experimental findings demonstrate that the adsorption heating and isosteric remain larger in the parentally Maxsorb 3/ethanol combination, the adsorption capacity rises in $H_2$-treated Maxsorb 3, and the adsorption kinetics accelerate in KOH-$H_2$-treated Maxsorb 3. Theoretically, an $H_2$-treated Maxsorb 3/ethanol adsorptive refrigerator machine can reach a 0.51 (COP) and around 374 kJ/kg (SCE) with an evaporator temperature of (-5°C) and (100°C) regeneration temperature and ambient temperature of (30°C).

Miyazaki *et al.,* (2014) examined a single-bed adsorption-cooling machine by using simulation to reduce the size of adsorption cooling systems used in air conditioning and refrigeration. The investigation uses the activated carbon powder-ethanol pair's adsorption isotherm and adsorption kinetic data. To obtain the optimum specific cooling power, the time parameters of the four adsorption/desorption cycles. The findings demonstrated that to achieve the maximum SCP, the adsorptive period must take more than the adsorptive period. With (80°C) for hot water, (30°C) for cooling water, and 14◦C for chilled water, the simulation predicted 140 W/kg (SCP) and 0.48 (COP). The same group of researchers (Uddin *et al*., 2014) measured the ethanol adsorption isotherms of $H_2$-Maxsorb III and KOH-$H_2$-Maxsorb III experimentally by using a magnetic suspension adsorption technique. Thermodynamic investigation reveals that at a generation temperature of 100°C, the $H_2$-Maxsorb III/ethanol adsorption cycle may reach a COP of up to 0.58. By adding a coolant at (30 °C beneath 100 °C), the KOH-$H_2$-Maxsorb III/ethanol combination may reach COP 0.56

Umair *et al.,* (2014) investigated the integrated design of an adsorption cooling structure employing simulation. A compound parabolic concentrator (CPC) with wing-model is used in the simulation research of an adsorptive cooling unit energized by solar energy. The machine is constructed from a refrigerator, a generator adsorption bed, a condenser, and a collector with wing kind angled at ideal distances. According to the modeling simulated results, the comparison performance coefficient between a linear CPC with a collector has an equal length, and the machine performance having a winged-model CPC rises by up to (6%) in the summer and up to (2%) in the winter. With the wing-type CPC, ice production rises by up to 13% throughout the summer.

Dakkamaa *et al.,* (2015) examined the effectiveness of several adsorbent/adsorbate working pairs in cascade adsorption cycles using the Matlab–Simulink program. The two pairs of adsorption beds, a condenser, an evaporator, and an integrated condenser/evaporator heat exchanger form an upper circuit and a lower circuit in this cascade system. (ATO-ethanol + Maxsorb/R507A), (Maxsorb/R134a + Maxsorb/propane), (ATO/ethanol + Maxsorb/propane), and (Maxsorb/R134a + Maxsorb/R507A) were the four combinations of operating pairings that were examined. The study working pairs' performance was assessed in terms of cooling capacity. The results showed that the Maxsorb/R134a + Maxsorb/Propane combination resulted in notable improvements in COP and cooling capacity of up to 30.0% and 30.1%, respectively, when compared to the reference version.

Frazzica *et al.,* (2016) made a functioning generator bed pair (SRD 1352/3) of ethanol and activated carbon was tested on a new, miniature prototype adsorption refrigerator. A gravimetric large temperature jump (G-LTJ) instrument was used to analyze the experimental data. According to the test findings, the air conditioning and refrigeration systems had high specific cooling capacities (SCPs) of 95 W/kg and 50 W/kg, respectively, with COPs ranging from 0.09 to 0.11.

Bouzid *et al.,* (2016) assessed the physical properties of ethanol adsorption, and utilization, of three different kinds of activated carbon: Maxsorb 3, which was the beginning carbon, and two chemically, modified activated carbons (KOH-$H_2$-Maxsorb 3 and H2-Maxsorb 3). The findings demonstrate that the ethanol molecules were adsorbed at locations that were either perpendicular to or non-parallel to the adsorbent's external surface.

To achieve a coefficient of performance (COP) of 0.6, (Saha**,** *et al*., 2006 and 2007) showed that the ACF-ethanol adsorption cooler may attain a constant periodic steady state after three half cycles, or 1890 seconds, for a system that employed ethanol and activated carbon fibers as a working pair, independent of the starting mass distribution. The temperature range of the heat source was set at around (60 to 95°C), and the cycle periods were set to 600 to 700 seconds.

disclosed that, regardless of the initial mass distribution, for a system that used ethanol and activated carbon fibers as a working pair, the ACF-ethanol adsorption cooler may reach a constant periodic steady state after three half cycles, or 1890 seconds. Heat source temperatures were adjusted to range from around (60 to 95°C), and cycle times were set at 600 to 700 seconds. Then. The results of the simulations showed that the power supply temperature range of 80 to 85°C produced the highest (COP). This suggests that the refrigerator performs very well and is a good fit for recovering waste heat at low temperatures.

Shabir *et al.* (2020) explored the basic adsorptive systems characteristics performance of 8 pairs of activated carbons with refrigerants. For cooling and refrigeration applications, the evaporation temperatures are chosen to be (7 °C and −5 °C), correspondingly. The (Maxsorb-III/methanol) pair was found to exhibit the maximum coefficient of performance and specific effective cooling energy over a broad fluctuation of initiation temperatures. The COP cycle and SCE at a desorption temperature of (80 °C) are 639.83 kJ/kg and 0.803, respectively. The potassium hydroxide subjected to phenol resin sphere treatment (KOH6-PR/ethanol) and (WPT-AC/ethanol) pairs similarly provide excellent performance analogous to the (Maxsorb-III/methanol) pair.

To address the sporadic behavior and enhance the subpar efficiency of single-bed adsorption refrigeration systems. A dual-bed generator solar adsorptive cooling machine was suggested as a solution to the sporadic nature of single-bed systems. By using, a pair of AC/ethanol, (Sha and Baiju 2021) conducted a thermodynamic investigation to examine the 2-bed solar adsorptive refrigerator performance machine. The study selected a 500 W cooler with 278.3 °K, evaporation temperature, and a condenser temperature of 318.3 °K. The system's pressure of evaporation is 201 Pa, whereas the pressure of condensation is 2310 Pa. The maximum coefficient of performance (COP) of 0.68 was recorded when the desorption temperature reached (95 °C).

To enhance the functionality of a comparable line of solar adsorptive units, Denzinge *et al.,* (2021) developed, constructed, and conducted experiments on a prototype that utilizes ethanol and activated carbon, which are often employed eco-friendly substances, as the primary elements of a solar-power-driven adsorptive cooler. The temperatures on the exterior wall of the vacuum tube in the solar adsorption refrigerator prototype ranged from 2 to 8°C. The findings demonstrated that one could achieve annual savings corresponding to a Global Warming Potential (GWP) reduction of 292 to 1170 kg of $CO_2$.

For the use of solar adsorption systems in heat pump applications using ethanol as an adsorption environment refrigerant with zero globing warm (GWP), Hasan Rupam *et al*., (2023) experimentally investigated, the amount of ethanol adsorbed on 3 dissimilar metal-organically structures (MOFs), with different temperature of evaporator. The conducted data from experimental isotherm are correlated with two models of isothermally adsorption, (Dubinin-Ashtakov. (DA) or Dubinin-Radushkevich. (DR).

Sghaier *et al.,* (2022) compared thermodynamic analysis of two different adsorbate/adsorbent pairs with two different consecutive adsorption-cooling cycles. Ethanol/waste-palm trunk and ethanol/mangrove-wood. Then, use statistical physics methods to calculate the COP of the adsorptive cooler machine. The outcome proved that the second system (ethanol/M-AC) showed the highest COP (0.81) (based on isothermal adsorption).

Kalawa *et al.,* (2023) showed how fluidized beds might be used in adsorption chillers. This study presents simulations of the bed temperature profiles throughout the adsorption and desorption processes of sorbent in a fluidized bed, as well as the findings of CFD numerical modeling of the operation of a fluidized bed for an adsorption chiller.

In Iraq, studies have been conducted to explore the efficacy of utilizing a working couple, the AC with methanol within a solar adsorptive-cooling unit. These investigations involved experimental analyses, design considerations, and the construction of prototypes and field systems aimed at assessing the feasibility and functionality of this configuration within the Iraqi context. These efforts aimed to harness solar energy through adsorption-based refrigeration systems utilizing methanol-activated carbon pair, displaying potential advancements in sustainable cooling technologies tailored to the country's needs and resources (Farman *et al.,* 2017 and H Al-Maamory & Fadel Farman 2023).

With a similar goal of optimizing the performance of ethanol solar adsorption units, the literature review shows that alternative advanced cooling systems and adsorption, cooling technologies are essential practical options that overwhelm the shortcomings of conventional adsorption machines. Research that is both theoretical and experimental has been conducted about the adsorption refrigeration system. The solutions may be done by using different working operating pairs, design sizes, and heating resources. The results obtained with different working pairs vary depending on the operating environment. Research on activated carbon-based adsorption systems is important compared to other machines. The literature review similarly demonstrates that the coefficient of performance for adsorptive machines may be sometimes lower compared to traditional structures and the performance needs to be improved. Moreover, there appears to be relatively little research into adsorption refrigeration systems, especially with ethanol as an adsorbate in Iraq.

## 3. System Description and Operating Principles

Typically, a solar adsorption refrigerator unit comprises three primary apparatuses: a solid generator bed, containing activated carbon. The condenser-part and an evaporator part. The process begins with closed valves linking the evaporator-generator bed, whereas working fluid remains condensed within the system. At this stage, both the adsorbent bed and the evaporator sustain low vacuum pressures and temperatures while being charged with the refrigerant. Figure 1a. Shows the typical schematic solar adsorption refrigerator unit. For the present, study the geometrical design of a single-bed generator with the evaporator, condenser, and solar collector is shown in Figure 1b.

Upon opening the valves, the working fluid vaporizes, initiating a cooling effect within the system. This evaporation process serves distinct purposes based on the intended application, which has been categorized into three groups: freezing, refrigeration, and air conditioning. Each application aligns with specific temperature and cooling requirements, allowing for tailored utilization of the working vapors to suit the desired cooling purpose.

However, it is essential to note that adsorption-cooling technologies have been commonly criticized for their relatively lower performance compared to traditional refrigeration methods. This lower performance is often highlighted as a

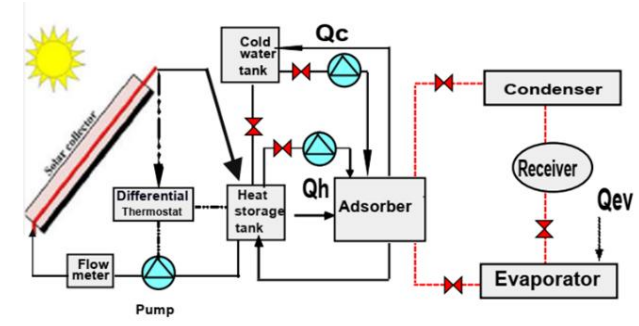


(a)

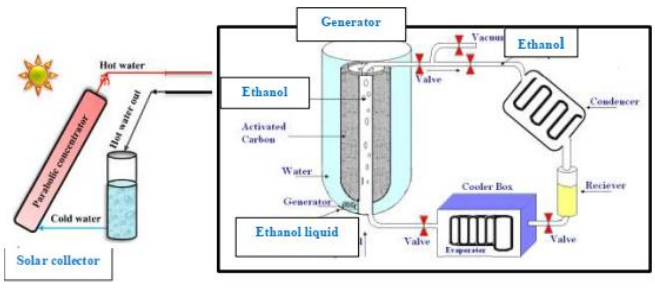


(b)

**Fig.1** (a) A basic adsorption intermittent cycle schematic diagram, (b) Diagram representing the standard solar adsorptive cooling machine

**Table 1**
Ethanol (ethyl alcohol) (C2H5OH): properties

| Properties | Value | Unit |
|---|---|---|
| The nominal boiling point | 78.24 | °C |
| The Tripple point | -114.15 | °C |
| The density | 785.47 | Kg/m3 |
| The molecular weight | 46.068 | Kg/mol |
| The critical temperature | 240.75 | °C |
| The critical pressure | 6.148 | Mpa |

significant drawback of adsorption cooling technologies. Lache *et al* (2023) improved the performance by using wasted heat and natural refrigerant water, adsorption chillers to reduce the amount of greenhouse gas emissions associated with both energy-related and refrigerant leakage-related conventional cooling technology. By using, Ethanol as boiling antifreeze in adsorption chillers as a workaround for this restriction. the adsorption chillers can operate below (0 °C).

Uddin *et al.,* (2013) proposed desorption–compression hybrid refrigeration systems with two various cycle configurations, cascade type and subcooled type. Ethanol/activated carbon is utilized for the adsorption part.

Despite their eco-friendly refrigerant characteristics, the efficiency and performance levels of adsorption cooling systems are aspects that require continued development and improvement to make them more competitive with conventional cooling technologies (Boruta *et al.,* 2021). The efficiency of activated carbon with ethanol as a compatible combination in adsorption refrigeration cycles has previously been evaluated. Therefore, extra research is required to examine how it might be used in multiple-bed generator adsorption units operated by solar energy. The cycles might have an isothermal process of adsorption rather than an isobaric one. The uptake behavior of ACF (A-20) seems to be a favorable pair for adsorption cooling applications (Saha *et al.,* 2006 and Frazzica *et al.,* 2016). Table 1 describes ethanol properties.

### *3.1 An Explanation of the Solar Adsorption Refrigerator's*

The solar energy adsorption cooling process involves substituting the traditional steam compressor electrical system with a natural source of thermal energy, for example, solar radiation energy imitative by the sun. There are four processes in the system's operational cycle, as displayed in the Clapeyron chart in the figure. 2. (1-2) the preheating-process, and (2-3) the desorbing-process together comprise quasi of the system cycle, while (3-4) the precooling and (4-1) adsorption processes constitute another part. Throughout the phase of reheating, the generator reactor (bed) captures solar energy, resulting in a rise in temperature for both the adsorbent (e.g., AC, zeolite, silica gel) and (e.g., methanol, ethanol, and water) for example adsorbate. The four operating cycle procedures are described below:

- Route (1-2) Isosteric heating: preheating of the adsorbent/ bed generator, and the adsorbate, at a fixed concentration of the adsorbate ($x_{max}$), and consequently, the process of adsorptive happens. The AC, ethanol, and metal parts of the bed generator are heated using the heating collected from solar radiation. Once bed-pressure rises to match the condenser pressure, consequently, the valves connected to the bed should be closed.
- Route (2-3) Isobaric heating: desorption route at condensation pressure. After the conclusion of this desorption process, the dilution of the adsorbate in the generator reactor (bed) attains the lowest value, denoted as $x_{min}$. Then once the adsorbent material achieves the highest temperature that is necessary, the adsorbate, which is caused by the high-pressure differential, is released to the condenser, where it condenses.
- Route (3-4) Isosteric cooling: pre-cooling. Subsequently, the fluid phase adsorbate moves through the condenser towards the evaporator. The temperature of the adsorbent bed during this procedure is reduced and reaches evaporation pressure after slowdown solar radiation and cooled by ambient temperature.
- Process (4-1) Isobaric Cooling: through an adsorption, process occurring at the pressure of the evaporator. At the evaporator pressure, at that moment the regulative-valve ahead of the evaporator opens. The adsorbate in the evaporator captivates the heating of water then evaporates and is adsorbed by the bed. Consequently, the liquefied water in the evaporator converts chilled otherwise completely or partly ice-transformed before, the reheating and cooling procedures are conducted with a consistent uptake of the adsorbate. Finally, the adsorbate concentration ratio fluctuates during the cycle (Alamoudi *et al,* 2021).

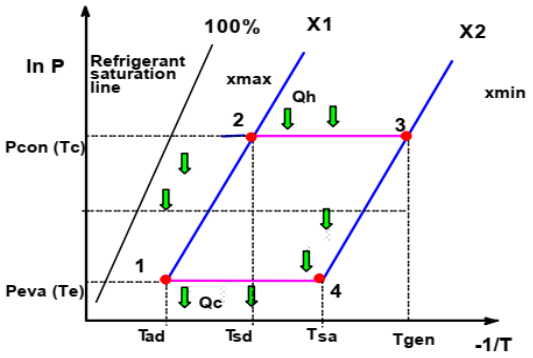


**Fig. 2.** The cycle diagram of the adsorption cycle.

### *3.2 The principal operation of the present case of solar adsorption*

The discontinuous nature of a basic-bed adsorptive cooling machine results in reduced performance. To get around the single-bed system's erratic performance, a dual-bed solar continuous adsorption-cooling machine is suggested as shown in the Figure. 3. The system's two primary circuits are a refrigeration system and a solar-energized collector with a receiver. The refrigeration structure consists of two beds of adsorbent as generators, a condenser, a throttling regulator-valve, and an evaporator. The collector-receiver apparatus contains a flat plate solar-collector, receiver, and water tank.

The purpose of the solar collector is to gather solar radiation and heat the water that is passing through the adsorber bed. The adsorbent bed has an inner chamber, which has enough activated carbon in it to adsorb the charged refrigerant ethanol. The evaporation latent heat enthalpy is used for cooling water, by the refrigerant mass accumulated. Moving hot or cold water over and done with the bed, causes a change of generating temperature. Fig. 4 shows the diagram of the current solar adsorptive refrigerator unit. The bed generator contains AC to adsorb ethanol. 8 valves regulate the processes of the desorption/adsorption period, causing each generator bed to function sporadically. For the desorption process, valves V5, V1, V6, & V3 are unlocked, and regulative-valves V2, V7, V8, & V4 are open for the process of adsorption. Adsorption Bed 1

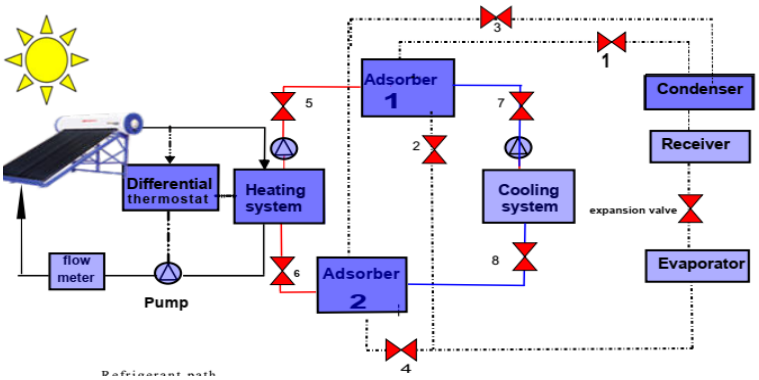


**Fig. 3.** Representation Diagram of 2-bed solar Adsorptive Refrigerator machine

receives evaporated refrigerant from the evaporator, which flows to the bed when the desorption process is taking place. If not, the released gaseous refrigerant must flow to the condenser. Every bed will execute a separate operation at different intervals to allow the evaporator to cool down.

The system involves two beds, with sporadic heating and cooling operations applied to each bed. Heating-route Bed 1 and cooling-route Bed 2, with generator Bed 1 in saturated ethanol and generator Bed 2 in the adsorption phase, can operate the structure. The condenser, as well as the evaporator, have refrigerant at an operational level. V5 and V1 are opened and V7 and V3 are closed at the beginning of the process desorption phase in Bed 1. So saturated ethanol vapor will travel to the condenser and is liquefied by cooling water. Condensed liquid enters the evaporator through the expansion valve; somewhere it takes up the heat evaporation from the water and evaporates. After that, V4 and V8 are opened to let Bed 2 adsorb the evaporator's vapor. After the adsorption process is finished, the cycle is finished, and the new cycle is initiated by heating bed 2 and reversing the previous process. By opening valves V7 and V2, Bed 1 initiates the adsorptive process and Bed 2 operates in the desorption phase during the subsequent cycle, which results in a continual cooling effect in the system. Valves 5, 6, 7, and 8 control the hot or cold water stream toward the generator beds. Hence, in contrast to an intermittent adsorption refrigerator machine, a continuous cooling process may be achieved with this system. The system is powered by solar energy, which is used via a solar collector to heat the water, making it a more environmentally friendly system. Table 2 describes the state of the valve and the water flow throughout the bed cycle. (Saha *et al.,* 2006 and Alamoudi & Abdel-Dayem, 2021**)**

## 4. Thermodynamic analysis methodology

The performance of the intermittent adsorption refrigerator machine is suboptimal. A solar adsorptive cooler machine with 2 beds is suggested as a solution to address the issue of intermittency found in single-bed systems. The simulation studies on 2-bed adsorption refrigerator systems are the main emphasis of this paper to product cooling effects energized by solar energy. The simulation modeling considers the bed, evaporator, condenser, and characteristics other than (AC/Ethanol) working–pair properties concerning environmental circumstances.

The following presumptions are used to model and examine the transmission of mass and heating processes in the generator bed:

- The adsorbent is made up of uniformly sized particles, and the bed is uniform with constant sponginess.

**Table 2**
Conditions of the valve connected with the two beds during the operation

| The phase of the system | Position of connected valves with the two beds | | |
|---|---|---|---|
| | Evaporator | Condenser | Hot/ Cooled Water |
| Adsorption | Open | Closed | Cooled |
| Preheating/Cooling time for bed | Closed | Closed | x |
| Desorption | Closed | Open | Hot |
| Preheating/Cooling time for bed | Closed | Closed | x |

- The uniformity of pressure, temperature, generator bed, and amount of ethanol adsorbed is ensured.
- The adsorption process occurs with variable adsorbent bed pressure and constant ambient temperature.
- The vapor of ethanol acts as a perfect gas whereas the adsorbing state is a liquid.
- The thermal specifications are stable with the temperature for all metal apparatuses.
- The two phases of adsorption/desorption for ethanol happen in the vapor state.
- At the same point, the temperature of activated carbon and ethanol is identical.
- No leakage heat.
- To prevent heat loss from the outside, the condenser, the unit machine, and the evaporator are all properly insulated.
- Within the porous bed, convection effects are minimal.
- Because the adsorber bed wall is thin and homogenous, the temperature and thermophysical characteristics will be constant at every site.
- Because of the condensation vapor filled the adsorbent porous resurfaces, the desorption/adsorption ethanol-specific heat is equal to that of the substance liquidized ethanol.

### *4.1 Equilibrium Ethanol Adsorption Uptake*

In the existing solar adsorption model, using the (D-A), equation of Dubinin-Astakhov for assessing ethanol uptaken of AC-ethanol couple. It characterized the concentration of refrigerant within the pores of the adsorbent (Burchell 1999)

$$X(P,T) = X_0\,[exp\{-D(Tln\tfrac{P_S}{P})^n\}\,] \quad (1)$$

$$X(T,T_{Sat}) = X_0\,[exp\{-K(\tfrac{T}{T_{Sat}}-1)^n\}\,] \quad (2)$$

With an assumed density of adsorbed phase r, the mass concentration x can be linked to the volume of the adsorbed phase as follows: x=ρv, At temperatures above critical, the value of refrigerant can be connected to supercritical properties or calculated as that of a saturated liquid at the same temperature. It is possible to confirm the volumetric fraction phase of refrigerant during a steady state by:

$$\theta = X(T,P)(1-\mu)\frac{\rho_{ac}}{\rho_{leth}(T)} \quad (3)$$

Where γ and $\rho_{AC}$ are the solid adsorbent's material density and total adsorption bed porosity, in that order.

The mass of ethanol (refrigerant) adsorbed per mass of activated carbon (adsorbent) is represented by the symbol X(P, T) (kg/kg). The adsorbent bed's pressure (P) and temperature (T) determine this value. The maximal or saturation adsorption capacity, or $X_0$, is determined by the structural constant (D) unique to the combination of adsorbent and refrigerant. The adsorbate saturation pressure at the evaporation pressure of ethanol is denoted by $P_{Sat}$, at $T_{Sat}$, whereas P denotes the equilibrium pressure of the adsorbent-refrigerant combination. The particular adsorbate-adsorbent combination and the adsorbent material's microstructure affect the coefficient of affinity, D, or the ethanol dilution on AC at equilibrium( X ).

When the refrigerant is removed from or added to the bed, the cooling effect achieved by solar adsorption refrigeration system by four processes: (a) isosteric heating, (b) isobaric heating (desorption process), (c) isosteric cooling, and (d) isobaric cooling (adsorption process), as seen in Figure 3. The energy balance equation utilized for the thermodynamic mathematical modeling of the system is derived from the aforementioned processes. The simulation work utilizes the starting point parameter as specified in Table 2. In addition, the D-An equation for the activated carbon-ethanol system utilizes a constant, denoted D, with a value of (1.716 x $10^{-6}$ $K^{-2}$), ( $X_0$ = 0.797 kg/kg) and the value of n is two. The saturation property of ethanol is obtained via the EES software.

### *4.2 Isosteric Process of Heating 1—2*

The adsorbent bed is heated throughout this procedure while maintaining a steady dilution of adsorbate ethanol in the bed. Absorbing heating by the solar collector, from solar radiation is added to the system. Total heating added $Q_{1-2}$ are the ethanol sensible heats, metallic wall (tube &shell), plus activated carbon, respectively. The sensible heat of the bed reactor parts could be transcribed as:

$$Q_{1-2} = \left(Q_{tube_{1-2}} + Q_{shell_{1-2}} + Q_{A.C._{1-2}}\right) * (T_{sd} - T_{ad}) + Q\_eth_{1-2} \quad (4)$$

Where the sensible heats of metal (tube &shell), and activated carbon are:

$$\Delta U_{tube} + \Delta U_{shell} + \Delta U_{A.C.} = (m_{tube}.c_{tube} + m_{shell}.c_{shell} + m_{A.C.} * c_{A.C.})(T_{sd} - T_{ad}) \quad (5)$$

The change in internal energy of ethanol is:

$$U_{(eth)_{1-2}} = m_{eth} * \left(U_{eth._2} - U_{eth._1}\right) \quad (6)$$

The specific interior energy of liquid ethanol at this position $U_{eth._2}$&$U_{eth._1}$ could be established way using the EES programming, employing two thermodynamic properties, denoted, the wetness portion), and the saturated temperature. Since $\frac{T}{T_{sat}}$ is constant lengthwise an isosteric process, $T_{sd}$ can be found by:

$$\frac{T_{ad}}{T_{eva}} = \frac{T_{sd}}{T_{con}} \quad (7)$$

$$Q_{1-2} = (m_{tube}.c_{tube} + m_{shell}.c_{shell} + m_{A.C.}.c_{A.C.})(T_{sd} - T_{ad}) + m_{A.C.}.x_{max}.\left(U_{eth._2} - U_{eth._1}\right) \quad (8)$$

### *4.3. Isobaric Process of Desorption 2—3*

During this stage, the bed generator is under a desorption period at the pressure of the condenser. This causes the absorption by the adsorbate ($x_{max}$) in the AC to fall to its lowest value ($x_{min}$). During this operation, the total heat entering ($Q_{2\rightarrow3}$) is calculated by the heating added to the activated carbon bed adsorbent, the metal (tube & shell), and the adsorbate ( $Q_{2-3} + Q_{des}$ ). This process is endothermic. The heat generated in this process can be expressed as follows:

$$Q_{2-3} = m_{A.C.}.\Delta x.h_{ad} + m_{A.C.}.\Delta x.\left(U_{eth_3} - U_{eth_2}\right) + (m_{tube}.c_{tube} + m_{shell}.c_{shell} + m_{A.C.}.c_{A.C.})\left(T_{gen} - T_{sd}\right) \quad (9)$$

The general energy balance equation through a control volume C.V. with no work done will be:

$$\delta Q = \sum m_e\, h_e - \sum m_i\, h_i + \delta\dot{Q} + dU_{CV} \quad (10)$$

During the desorption, and adsorption process, the saturation pressure reached $P_{con}$ and $P_{eva}$ respectively.

H represented the heating of the desorption heat /mass of ethanol (kJ/kg). For any point, can be predictable through the desorption/adsorption pathway from the slope of the line (1–2) or line (3–4) in Figure. 2. (Burchell, 1999) as the following:

$H = R\left[\frac{\partial(ln[P])}{\partial(\frac{1}{T})}\right]_x$, where R, is the gas constant of ethanol and can be evaluated from the latent heat of ethanol

$$H = L_{eth}(T/T_{sat}) \quad (11)$$

$$dH_{eth._e} = h_{eth._e}.dm_e \quad (12)$$

$$h_g = h_{eth._e} = enthalpy\left(ethanol, x=1, T=\frac{T_{sd}+T_{gen}}{2}\right), h_{eth._e} = m_{A.C.}.\Delta x.h_g \quad (13)$$

The middling heating of adsorption may be considered as follows:

$$h_{ad} = R\,.\left(A\left(\frac{T_{sd}+T_{gen}}{2}\right) - ln\,P_{con}\right) \times \frac{T_{sd}+T_{gen}}{2} + \frac{R(A(T_{sd}) - ln\,P_{con})T_{sd}}{2} + \frac{R(A(T_{gen}) - ln\,P_{con})T_{gen}}{2} \quad (14)$$

$A = \left[\frac{\partial(ln[P])}{\partial(\frac{1}{T})}\right]_x$, The augmentation in interior energy of the control volume is:

$$\Delta U_{tube_{2-3}} + \Delta U_{shell_{2-3}} + \Delta U_{A.C._{2-3}} = \int_2^3 (m_{tube}.c_{tube} + m_{shell}.c_{shell} + m_{A.C.}.c_{A.C.})\,dT = (m\_tube.c\_tube + m\_shell.c\_shell + m_{A.C.}.c_{A.C.})(Tgen - Tsd) \quad (15)$$

$$Q_{des} = m_{A.C.}.\Delta x.h_{ad} \quad (16)$$

The alteration of the internal energy of ethanol can be initiated by employing the following equation:

$$\Delta U_{eth._{2-3}} = \left(m_{A.C.}.x_{min}.U_{f_3} - m_{A.C.}.x_{max}.U_{f_2}\right) \quad (17)$$

The production or regeneration energy is the total of the isosteric and desorption heat) and can be expressed as follows:

$$Q_{in}^{1\to2\to3} = Q_{1-2} + Q_{2-3}$$

$$Q_{1-3} = Q_{1-2} + Q_{2-3}$$

$$Q_{1-3} = (m_{tube}.c_{tube} + m_{shell}.c_{shell} + m_{A.C.}.c_{A.C.})(T_{gen} - T_{ad}) + m_{A.C.}.x_{max}(U_{eth._2} - U_{eth._1}) + m_{A.C.}.\Delta x.\mathrm{h}_{ad} + m_{A.C.}.\Delta x.(U_{eth_3} - U_{eth_2}) \quad (18)$$

*4.4. Isosteric Process of Cooling 3—4*

This process from state 3 toward state 4, ($Q_{3-4}$) the heat rejected is analogous to the process from state 1 to state 2. Similar to the heating process, lines 3-4 demonstrate that the ethanol concentration ratio is constant but at the minimal concentration value ($x_{max}$). The bed is chilled to the temperature $T_{sa}$. In a hypothetical machine, there is a regulative-valve separating the bed from the evaporator that is now charged with the condensing ethanol.

$$Q_{3-4} = (m_{tube}.c_{tube} + m_{shell}.c_{shell} + m_{A.C.}.c_{A.C.})(T_{gen} - T_{sa}) + m_{A.C.}.x_{min}(U_{eth._4} - U_{eth._3}) \quad (19)$$

Where $T_{sa}$ may be calculated by:

$$\frac{T_{sa}}{T_{eva}} = \frac{T_{gen}}{T_{con}} \quad (20)$$

*4.5. Isobaric Adsorption Process 4—1*

The energy balance of C.V. Is:

$$\delta Q = dU_{CV} + h_e.dm_e \quad (21)$$

$m_e$, $h_e$ is the existing mass and enthalpy of saturated ethanol. One can consider the vapor coming out of the evaporator to be in the saturation state, which corresponds to the pressure of evaporation, $h_e$=$h_{ge}$. Thus, the accumulated mass of the ethanol at the start of the evaporation is:

$$m_{eth} = m_{A.C.}(x_{max} - x_{min}) = m_{A.C.}.\Delta x \text{ , Where } (x_{max} - x_{min}) = \Delta x \quad (22)$$

$$Q_{4-1} = (m_{tube}.c_{tube} + m_{shell}.c_{shell} + m_{A.C.}.c_{A.C.})(T_{sa} - T_{ad}) + m_{A.C.}.x_{min}(U_{eth._4} - U_{eth._1}) + m_{A.C.}.\Delta H.\Delta x \quad (23)$$

*4.6. Evaporation and condensation heat state*

The evaporator element produces cold through the evaporation of liquid ethanol. The following calculates the cooling production at the evaporator:

$$Q_{eva} = m_{A.C.}.\Delta x\left(h_{g_e} - u_{r_f}\right) \quad (24)$$

The evaporation heat can produce ice if the initial water temperature $T_{iw}$ falls below zero. The freezing water temperature and ice mass ( $m_{ice}$) are also determined using the following equations: (Burchell, 1999)

$$\mathrm{m_{ice}} = \frac{\mathrm{Q_{eva}}}{(\mathrm{L_{ice}} + \mathrm{c_w}(\mathrm{T_{iw}} - 273.15) + \mathrm{c_{ice}}(273.15 - \mathrm{T_{ice}})) + \mathrm{m_{eva}}\mathrm{c_{eth}}(\mathrm{T_{iw}} - \mathrm{T_{eva}})} \quad (25)$$

Mass of chilled water (Teva ≥ 0 °C): It can be expressed as, for air conditioning application

$$m_{cwc} = \frac{Q_{eva}}{c_w(T_{iw} - T_{eva})} \quad (26)$$

The condenser receives the ethanol vapor that was desorbed during the desorption phase. By extracting vitality from the superheating, vapor the temperature difference concerning the machine with surroundings. The ethanol vapor begins to condense when it reaches the saturated vapor state, losing its latent energy to the surrounding heat sink across a differential of $(T_{con} - T_{ambiant})$. The vapor is subcooled to the surrounding temperature after it condenses to liquid at $T_{con}$. The total heat rejected during the condensation process is given by:

$$Q_{con} = m_{A.C.}.\Delta x(L_{eth}) + m_{A.C}c_{eth}\int_{T_{con}}^{T_{gen}}(T_{con} - T).\left[\frac{\partial x}{\partial T}\right]_{P_{con}} dT \quad (27)$$

*4.7. Equilibrium of Energy throughout the Entire Unit*

The overall input energy ($Q_{added}$) and the output production ($Q_{rejected}$) to the unit can be computed by:

$$Q_{added} = Q_{1-2} + Q_{2-3} + Q_{eva} \quad (28)$$

$$Q_{rejected} = Q_{3-4} + Q_{4-1} + Q_{con} \quad (29)$$

*4.8. Performance Evaluation for Solar Adsorption Cooling System*

The proportion of cooling provided ($Q_{eva}$) to input heating ($Q_{added}$), required to heat the bed generator to the regeneration temperature $T_{gen}$, defines the performance coefficient (COP) and is derived from:

$$COP_{sys} = \frac{\mathrm{Q_{eva}}}{\mathrm{Q_{added}}} \quad (30)$$

$$COP = \frac{\mathrm{Q_{eva}}}{Q_{1-2} + Q_{2-3}} \quad (32)$$

The (SCP) of the machine and (COP) determine how well the adsorption refrigerator machine works. How effectively solar energy or heat added, ($Q_{added}$) is renovated to the beneficial cooling outcome ($Q_{eva}$). Then the cooling capacity (SCC), the specific cooling effect (SCE), and the specific cooling power (SCP) possible to write it as:

$$SCC = \frac{Q_{eva}}{Cycle\ Time * 3600} \text{ in } W, SCE = \frac{Q_{eva}}{m_{A.C}} \text{ kJ/kg} \quad (32)$$

Specific cooling power (SCP) differs amongst systems based on the system's capacity. Evaluated when chilled water is produced which, is used to calculate the effectiveness of an adsorption cooling system at various sizes. Defined as the proportion of the system's cooling capacity (SCC) to the mass of adsorbent in the adsorbent bed:

$$\mathrm{SCP} = \frac{\mathrm{SCC}}{\mathrm{m_{A.C}}} \quad (33)$$

$$COP = \frac{m_{A.C.}.\Delta x\left(h_{g_e} - u_{r_f}\right)}{\left((m_{tube}.c_{tube} + m_{shell}.c_{shell} + m_{A.C.}.c_{A.C.})(T_{gen} - T_{ad}) + m_{A.C.}.x_{max}(U_{eth._2} - U_{eth._1}) + m_{A.C.}.\Delta x.(U_{eth_3} - U_{eth_2}) + m_{A.C.}.\Delta x.h_{ad}\right)} \quad (34)$$

By measuring the refrigeration produced / unity mass of AC per unity time, for instance, specific cooling power (SCP) illustrates the size of the structure since it relates both to the mass of the adsorbent and the cooling power. This parameter reflects the size of the system. For a nominal cooling load, a higher SCP value indicates the stability of the system.

## 5. Results and Discussion

The current study focuses on an isobaric adsorption process-based solar-powered two-bed adsorption refrigeration system. The performance of the current system has been examined. The parameter taken into consideration for this work is provided in Table 3. The suggested cycle of a 2-bed solar adsorption cooler machine has been mathematically modeled and simulated in the EES. The thermodynamic properties of ethanol are imported from the EES program. The simulation of the approved computer code has been used to resolve the energy balancing equation intended for the evaporator, condenser, and bed. The simulation's results are summed up in the section that follows. Energy balancing is done for the entire system, which includes the condenser, evaporator, and bed. It was discovered that the system's total energy input added ($Q_{added}$) from the solar collector is equivalent to 11893 kJ, while the total energy output withdrawn ($Q_{rejected}$) is equal to 11845 kJ. As a result, the computations' relative error was roughly 0.4 which is a reasonably satisfactory valued error that confirms the analysis's accuracy. Furthermore, the machine achieves a round efficiency factor (COP) of 0.702 when its full refrigeration production ($Q_{eva}$) is 5169 kJ, and its total heat input ($Q_{input}$) is 7200 kJ. This two-bed solar adsorption system produces 39.4 kg of cold water at 5 °C using 16 kg of activated carbon for each bed. It produced 1 kg of chilled water for 2.463 kg of activated carbon at a temperature of (5°C). The specific cooling effect (SCE) is 161.5 kJ/kg; the cooling capacity effect (SCC) is 359.4 W and the specific cooling power (SCP) of 11.22 W/kg

Figure 4 shows how the system's sensible heat input is distributed throughout the bed's constituents. It is shown, that desorption heat from the majority part of the input heating absorption through isosteric heat. In addition, it is obvious that the metallic walls. Influence is insignificant.

**Table 3**
Values Adopted in the Cycle for EES Simulation Model (El-Sharkawy *et al* 2006, Saha, *et al* 2006 and 2007)

| The variable | value | The variable | value |
|---|---|---|---|
| Tgen | 95°C | D | 1.716 x10-6 /$K^2$ |
| Tcon | 45°C | X0 | 0.797 kg/kg |
| Teva | 5°C | n | 2 |
| Tad | 33°C | R | 180.48 Jkg-$1K^{-1}$ |
| Twi | 33°C | CA.C. | 0.711 kJkg-$1K^{-1}$ |
| Imax | 950W/$m^2$ | Ctube,Cshell | 0.480 kJkg-$1K^{-1}$ |
| Tambiant | 33°C | Ceth | 2.4 kJkg-1K-1 |
| ρwall | 7000 kg/$m^3$ | Cw | 4.2 kJkg-$1K^{-1}$ |
| ρA.C. | 2200 kg/$m^3$ | mA.C. | 16 kg |
| μ | 0.93 | Shell+tube | 16 kg |
| Cycle Power | 0.5 kW | | |

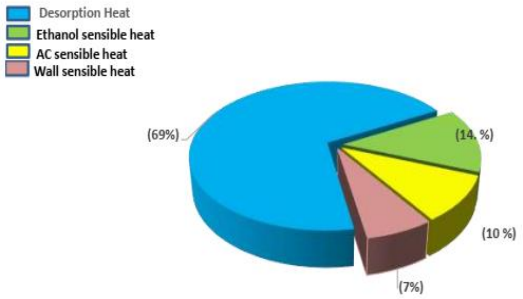


**Fig. 4.** Heat distribution throughout the bed's components

### 5.1 The Operational Parameters Influence

The engineering equation solver, EES program designed for thermodynamic analysis of the system's cycle parameters (as shown by Fig. 3) has been used to examine the impacts of the operative parameters ($T_{gen}$, $T_{ad}$, $T_{eva}$, $T_{con}$ $P_{con}$, $P_{eva}$, and $T_{iw}$) and the climate circumstances (Tambient, solar radiation) on the COP, SCP, SCC, SCE, x and the effective mass of circulated ethanol desorption). The maximum desorption temperature ($T_{gen}$) and the lowest adsorption temperature ($T_{ad}$) were the primary operational parameters that were the focus of the inquiry. AC, with ethanol with a starting concentration ratio of 0.797 kg/ kg, was employed with 16 kg for each bed to examine the impact of operating conditions on performance.

#### 5.1.1. Influence of Daytime on Ambient and Hot Water Temperature

The time of day has an impact on meteorological data, including solar intensity and atmospheric temperature, as depicted in Fig. 5. The daily maximum generation temperature and the time it occurs are determined by the day's weather. Baghdad's average sunrise and sunset times, which are 6 a.m. and 6 p.m., respectively, on a sunny day (March through June) aid in estimating the solar intensity and local ambient

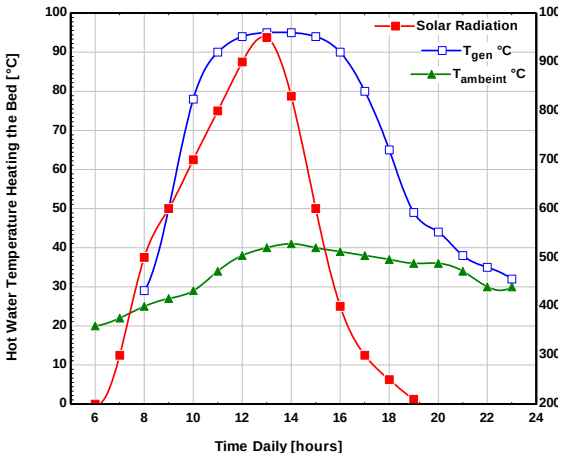


**Fig. 5.** Influence of daytime on ambient and hot water temperature

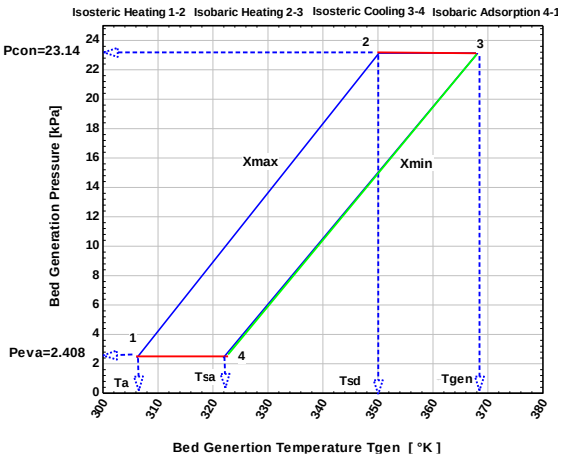


**Fig. 6.** The effect of bed generation pressure on bed temperature

temperature throughout the day (hypothetical clear day). The sun's intensity rises during the day from 200 to a maximum of 950 to 1000 W/m$^2$ between 12 p.m. and 1 p.m., after which it decreases to 100 until 6 p.m. After that, solar radiation is at zero intensity until the following morning at six a.m. starting around 6:00 am, a comparable trend is noted for the ambient temperature. Figure 5 also illustrates the variation in hot-water temperature throughout the day solar radiation. Throughout the day, by following the same pattern. This tendency is explained by the fact that sun intensity and water temperature are closely correlated.

*5.1.2 Adsorbent Bed Temperature-Pressure Relationship*

Fig. 6 shows the change in pressure of the generator bed according to bed temperature. The bed generation pressure increases beginning with evaporation pressure ($P_{eva}$) of 2.408 kPa until reaching condensation pressure ($P_{con}$) of 23.14 kPa during isosteric heating (1–2) where the maximum concentration of adsorbate ($X_{max}$). The refrigerant begins to start desorption when the bed hits 78°C, finally reaches the minimum concentration of ethanol ($X_{min}$), and continues until maximum generation temperature ($T_{gen}$=95°C). The isosteric cooling curve, or curve 3→4, displays a decreasing pressure trend. After this procedure, the lowest cycle pressure. The isobaric adsorption curve 4→1 shows the system's adsorption process at constant pressure.

*5.1.3. The effect of the generating temperature on cycle COP and cooling effect*

Fig. 7 displays the impact of the generating temperature on the cycle (COP) and cooling effect. This figure shows how the COP climbs quickly to achieve an optimal value that corresponds to an optimized temperature ($T_{gen}$). Furthermore, by way of the generation temperatures ($T_{gen}$) rising precisely above the optimal temperature value, the system's coefficient of performance (COP) begins to decrease. The refrigerating effect increases as the desorption temperature ($T_{gen}$) rises because internal refrigerant mass desorption also increases at this temperature. Thus, the system's COP rises to an ideal level and then falls below the ideal desorption temperature. More ethanol desorbed and cooling production come from higher generation temperatures, as seen in Fig. 7. However, this also causes more sensible heat loss from the bed, implying a rise in heat input.

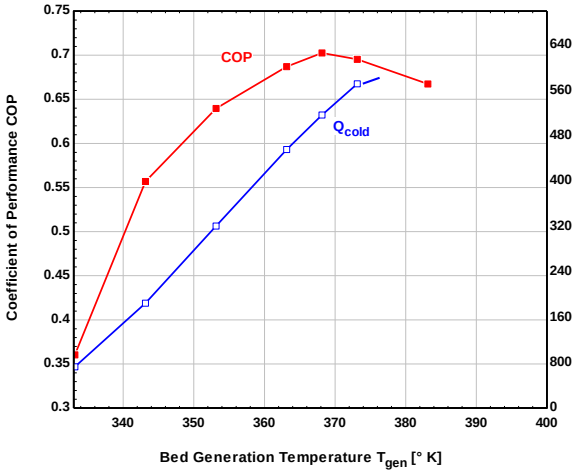


**Fig. 7.** The generating temperature influences COP and cooling effect.

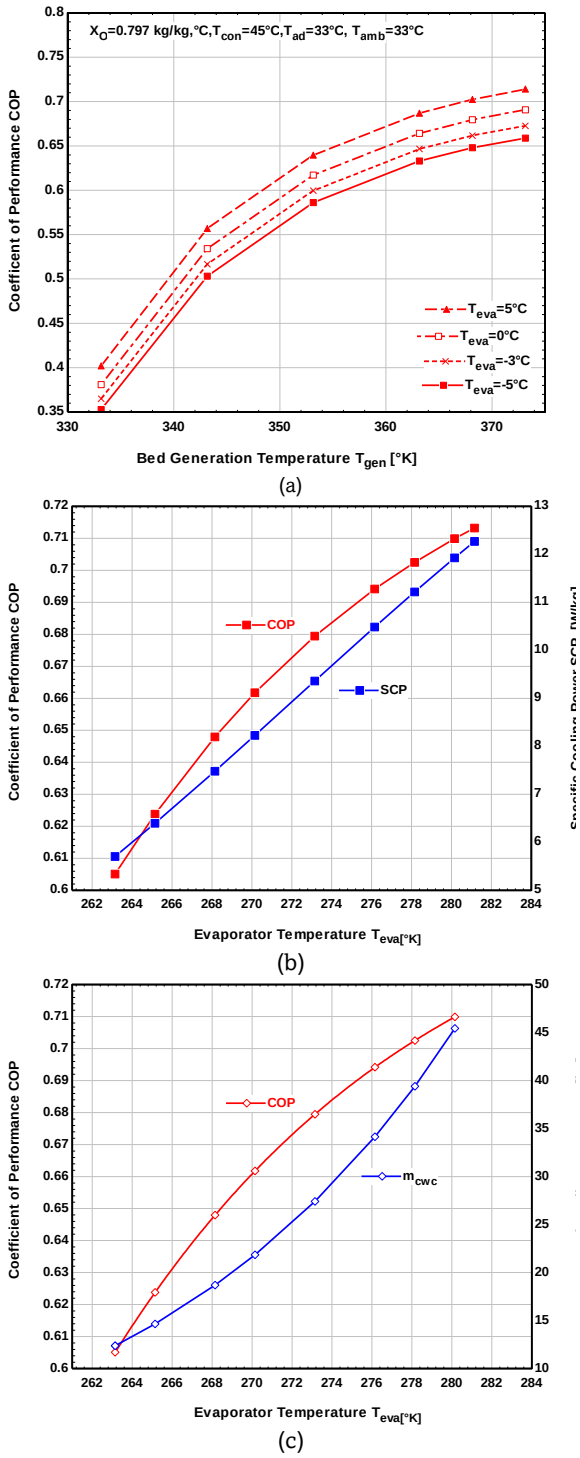


**Fig.8.** (a). Evaporation Temperature affects COP, (b) Evaporation Temperature affects COP and SCP, (c) Evaporation temperature affects COP and cold production

Moreover, the cycle COP deteriorates beyond the (350°K) temperature. This is because there has been a greater rise in heat intake than in cooling production (El-Sharkawy *et al.*, 2014 and Uddi *et al.*, 2014). For system performance, the activated carbon type selected influences the ethanol desorbed to gather upon cooling as the producing temperature increases.

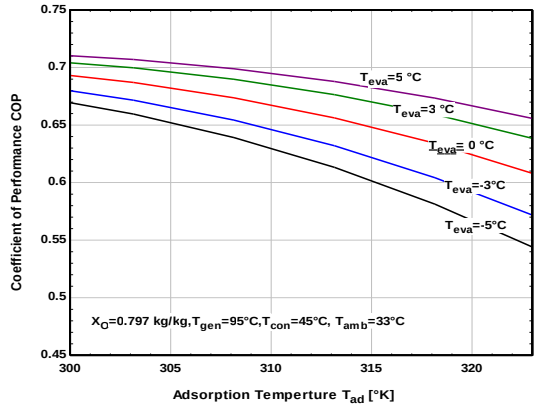


(a)

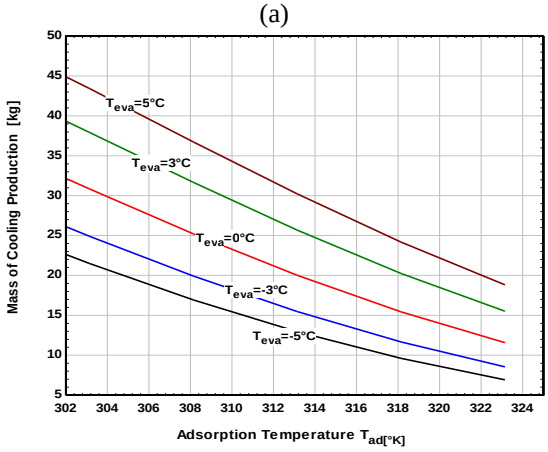


(b)

**Fig. 9**(a). Adsorption temperature affects COP; (b) Adsorption temperature affects cold production

*5.1.4. Effect of Evaporation Temperature on COP, SCP, and Cold Production*

The adsorption phase is accelerated by higher evaporator pressure, which causes an increase in ethanol cycled mass and, consequently, an increase in cooling production. As the evaporation temperature rises, so does the heat input from solar radiation, but at a slower pace than the cooling production, which improves system performance as illustrated in Fig. 8. These outcomes demonstrate a strong correlation with findings from the literature. Refrigerant evaporation provides a cooling effect through the adsorption phase. The evaporation procedure preserved the bed at condenser pressure. COP is dependent on generating temperature for activated carbon /ethanol with different Teva (-5 to 5 °C), wear displayed in Figure (8. a, b, and c). It is marked when the desorption temperature is (95°C), the increasing of COP noticeably employing rising evaporation temperature. Because increasing evaporation temperature indicates an increase in evaporation pressure. Nevertheless, even when the SCP rises to 11.22 W/kg, 39.4 kg daily production of cooling water product, the increase of COP above the desorption temperature of (95 °C) is quite slightly unnoticed. This occurs because the difference in temperature between the heating added and heating rejected rises above 50°K, and the need for heat input increases noticeably. $T_{eva}$ generally varies on the purpose of the use; for example, it is best to keep it between (-5 and -10°C) while manufacturing ice, although it can be raised to (5 and 8°C) when used for air-cooling and immunization storage, respectively. $T_{eva}$ is defined by the initial amount of ethanol adsorbed and the adsorption temperature for the sun cooling applications. Consequently, it makes sense to regulate the adsorption temperature, which is mostly determined by the ambient temperature in the area, to keep the evaporation temperature Teva within the necessary range. (Hadj Ammar *et al.,* 2017). When comparing the present $Q_{eva}$, 5169 kJ, with (Hadj Ammar *et al* 2017) which is equal, to 5026.45 kJ, it is clear the validation of the present mathematical model simulation.

*5.1.5 Adsorption Temperature Effects COP and Cold Production*

The performance is affected by the temperature of the evaporator and adsorbent. Since they operate simultaneously and have a direct impact on one another, just like the temperature of the condenser and desorption do. The performance is impacted in different ways by the evaporator and adsorption temperatures concerning the condenser and desorption temperatures, respectively, as illustrated in Figure 9. In Figure 9(a), the COP is plotted against the adsorption temperature (Tad) for a few chosen values of (Teva) between (-5 and 5) °C. The pattern indicates that the COP will first decline slightly as Tad ≤ 33°C increases, then sharply when the adsorption process time shortens. Because the process of adsorption takes place as soon as the bed generation pressure matches the evaporator pressure, the evaporator temperature is another crucial factor that greatly influences the system's effectiveness. As Tad increases, the volume of created cooling falls in an essentially linear pattern, as illustrated in Fig. 9(b). The system performs better when the evaporator temperature is higher since the adsorption temperature is lower at higher temperatures.

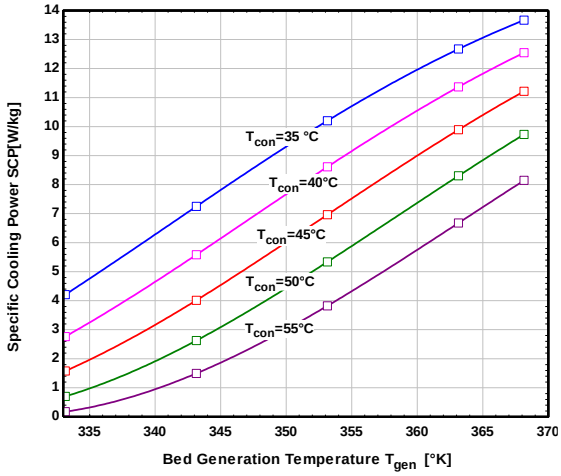


(a)

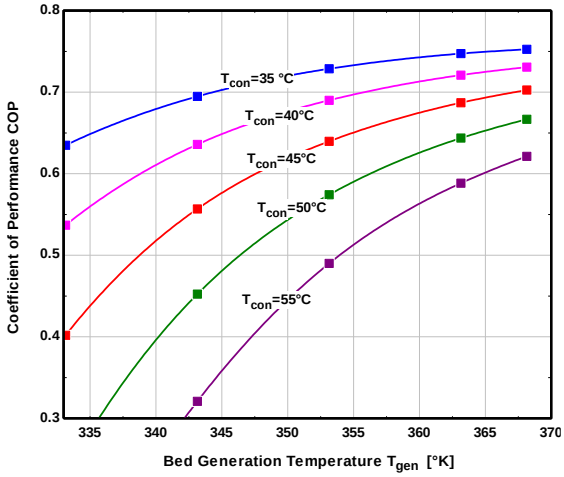


(b)

**Fig.10**. (a). Bed generation temperature effect COP, (b).Effect of the bed generation and condenser temperatures on the SCP

*5.1.6. Condenser temperature and pressure affect COP and SCP*

For a range of chosen condenser temperatures, while holding constant the other parameters, $T_{ad}$ (adsorption temperature), $T_{eva}$ (evaporator temperature), and $T_{iw}$ (initial water temperature) = 33 °C, Fig. 10(a) and (b) show an impact of the bed generation temperature $T_{gen}$ with the coefficient of performance (COP) and the cool providing ($m_{cwc}$), correspondingly. For any given condensation temperature higher than 25 °C, Fig. 10(a) illustrates a significant rise in the (COP) with the generation temperature range (70°C to 95°C). When $T_{con}$ is ≥ 35 °C, the COP is nearly constant for large values of $T_{gen}$ ($T_{gen}$ > 95 °C) and exhibits an almost linear, small decline with $T_{gen}$ for $T_{con}$ of ≥ 35°C. The majority of the ethanol had desorbed below 95°C, which is why the COP declines linearly with increasing heat input very little ethanol is produced. Likewise, raising the condenser temperature lowers the COP since it delays the desorption process. Furthermore, raising the condenser temperature lowers the COP since it delays the desorption process, which begins when the bed generation pressure reaches the condenser pressure. Fig. 10(b) plots SCP against the desorption temperature $T_{gen}$. The trend indicates a significant increase in cooling production with increasing $T_{gen}$ values for a certain $T_{con}$. At a fixed $T_{gen}$, the rate of increase in cooling amount with increasing generation, temperature values increase slightly based on the condenser temperature.

Fig.11 (a) illustrates how condensation temperature affects cycle COP and the system's total specific cooling power SCP; this figure shows that the condensation temperature is roughly equally influenced by the surrounding air temperature. The system's performance declines as the condensation temperature rises. This could be explained by the following: a rise in condensation temperature raises condenser pressure, which in turn delays the desorption phase and reduces the amount of ethanol that has been desorbed. This ultimately lowers the circulated mass of ethanol and the cool product. As the condensation temperature drops, the heat input will likewise drop, but not as much as the drop in ethanol cycled mass, which will result in a drop in COP. As opposed to the evaporation pressure.

Figure 11(b) demonstrates how raising the condensation pressure slows down the process of desorption and reduces the quantity of desorbed ethanol. Higher evaporation pressure values, as indicated in Fig. 6, can produce superior cooling effect outcomes because, in contrast to condenser pressure, evaporator pressure rises and hastens the adsorption process. (Qasem & El-Shaarawi, 2015).

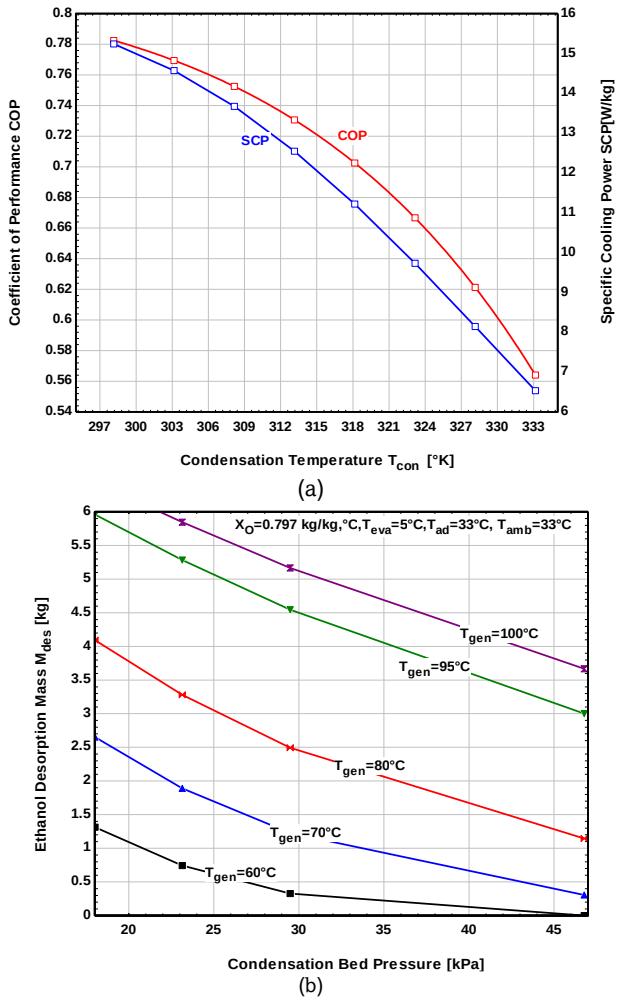


**Fig. 11.** (a) Condensation temperature affects COP & SCP, (b) Effect of the condenser pressure on the ethanol desorbed

*5.1.7. Evaporation pressure's impact on adsorption uptake*

Higher evaporator pressure values, as indicated in Fig. 12. Can produce superior cooling effect outcomes because, in contrast to condenser pressure, evaporator pressure rises and hastens the adsorption process. The adsorption phase is accelerated by higher evaporator pressure, which causes an increase in ethanol cycled mass and, consequently, an increase in cooling production. As the evaporation temperature rises, so does the heat input from solar radiation, but at a slower step than the cooling production, which improves the performance of the machine as clarified in Figure 8a. These outcomes demonstrate a strong correlation according to findings from the literature (Hadj Ammar *et al.,* 2017).

*5.1.8. The effect of bed generation temperature on uptake ratio and the volume fraction*

Analyzes the uptake of ethanol at equilibrium with ($T_{gen}$), shown in Fig. 13(a) A minimum ethanol concentration of $x_{min}$ equal to 0.12 kg/kg and $x_{max}$ equal to 0.39 kg/kg are recorded during this cycle, and the mass of ethanol is 1.92 kg and 8.24 kg, respectively. Consequently, 6.32 kg is the operative refrigerant mass cycling through this system, and 76 % is the productivity refrigerant of ethanol mass intake. For different ($T_{ad}$) can be verified that whenever decreases, desorption increases.

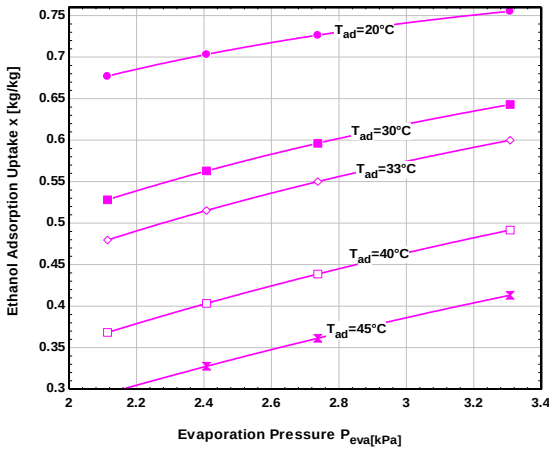


**Fig. 12**. Effect of the evaporator pressure on the ethanol adsorbed.

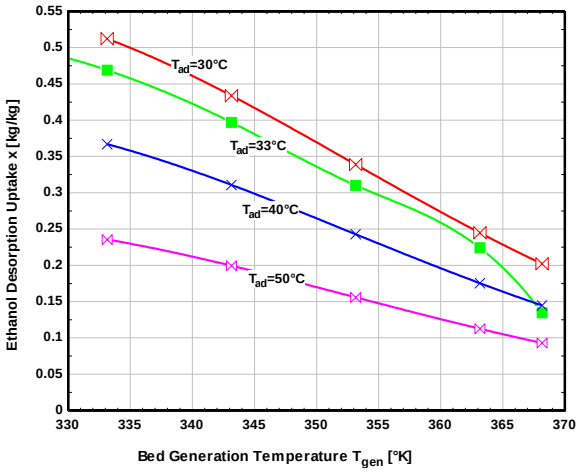


(a)

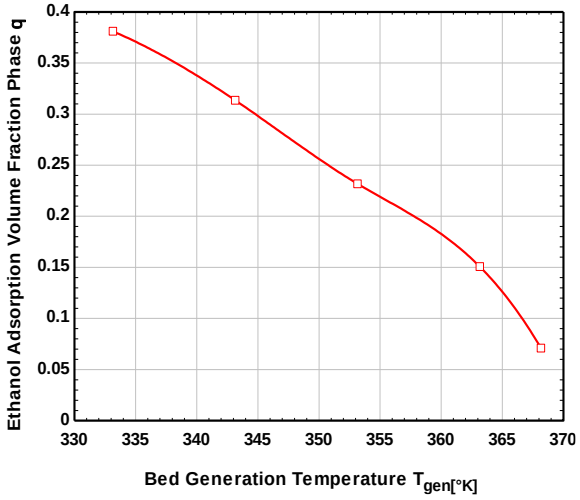


(b)

**Fig. 13.** (a) Adsorbate concentration ratio with bed generation temperature, (b) Adsorption volumetric fraction phase with bed generation temperature

Fig 13(b) contains the volume proportion of the adsorbate phase concerning cycle temperature. The volumetric fraction varies continually during the cycle, as demonstrated. There is a slight variation in (θ) of ethanol in both isosteric heating and cooling operations. Because of the drop in the density of adsorbed ethanol during the isosteric preheating route, the refrigerant (θ) rises as the temperature rises. Similar to this, as the temperature of the adsorbent bed drops during the isosteric cooling route, (θ) of the refrigerant reduces, as a result, the density of the ethanol rises. (θ) max, (θ) min acquired in the aforementioned procedures is thus found to be 0.37 and 0.088, respectively, from Eq. (3)(El-Sharkawy *et al.,* 2008).

*5.1.9. Variation in the desorbed and adsorbed refrigerant's affective mass*

Fig. 14. Shows the impact of bed generation temperature on the operative mass of ethanol desorbed for the period of the isobaric desorption route, (2→3). The proportion of desorbed ethanol from the bed generator extends its highest value during isobaric heating. The ratio of desorption rises constantly as bed temperature rises, reaching a minimum value at minimum concentration and a maximum at the end of this process.

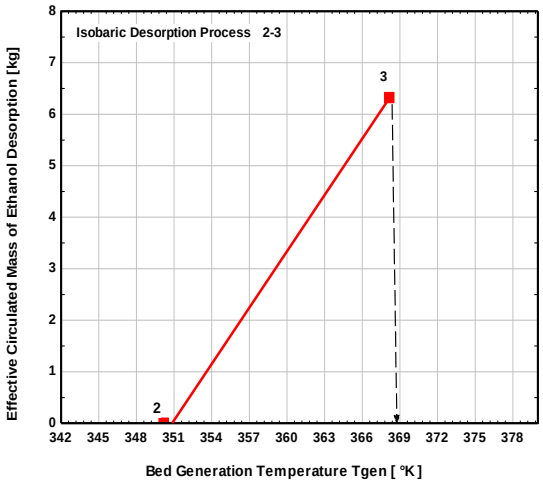


**Fig. 14**. Bed generation temperature affects the circulating mass of ethanol

*5.1.10. Bed pressure's impact with evaporator temperature on adsorption uptake*

Fig. 15. Shows how bed pressure affects activated carbon–ethanol adsorption uptake at constant adsorbent temperature. As demonstrated, at lower adsorbent temperatures, the adsorption uptake of ethanol by activated carbon rises with increasing pressure. As the temperature of the adsorbent increases, the adsorbate's capability falls. Therefore, it is better to keep the bed temperature as low as possible when it comes to adsorption. Cooling water at a low temperature can be circulated through the adsorbent bed to bring about this lower temperature. As a result, decreasing the temperature of the adsorbent bed increases the amount of adsorbate from the second bed that is adsorbed and adsorbate, improving the system's SCP and COP. To minimize the extra effort, the system has to undertake for the cooling process, it is, therefore, better to use tap water as the cooling medium after saving it in cooling storage for the adsorption bed and condenser under these operating conditions (El-Sharkawy *et al.,* 2008 and Saha *et al.*, 2016).

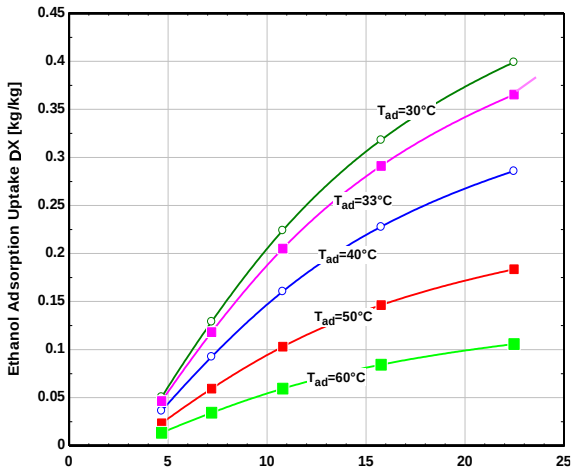


**Fig. 15.** Bed pressure's impact with different Teva on adsorption uptake

*5.1.11. Effect of Bed Generation Temperature on COP, SCP, Chilled Output Water Temperature, SCC, and Cooling Effect.*

Fig.16(a) displays the influence of the maximum bed-generating temperature upon the cycle, COP plus SCP. When the system is operating at a fixed ambient temperature, the COP gradually drops after first increasing with an increase in temperature of desorption and attainment of its maximized value. Inferred from other publications based on other adsorption methods (Sghaier *et al.*, 2023, Pal *et al.*, 2016, El-Sharkawy *et al.*, 2008).

The refrigerating effect increases as the desorption temperature ($T_{gen}$) rises because internal refrigerant mass desorption also increases at this temperature. As a result, the system's COP rises to an ideal level and then falls, surpassing the ideal desorption temperature. The energy utilized by the adsorber during this operation is used to increase the system's sensible heat. As a result, the shift in COP after it reaches an ideal value is gradual. At the highest ($T_{gen}$) of (95 °C), the average COP derived from the simulation is 0.702.

Figs. 16(b) and 16(c) depict, respectively, how the maximum desorption temperature affects the chilled-water outflow temperature and (SCP). Figure 7 makes it clear that for desorption temperatures between (80 and 95 °C), the cooling impact rises intensely from (800.4 k J to 3209 k J), lowering the temperature of chilled-water output. Nevertheless, the refrigeration effect gradually increases above (95 °C) since the temperature of dynamic input heat increases together using the ethanol amount desorbed. Increasing inlet hot water temperature leads to rises, and the chilling water output temperature drops, as shown in Fig 16c. Higher desorption temperatures cause additional adsorption of ethanol through subsequent cycles and then lower the temperature of the chilled water output because the ethanol vapor has desorbed more quickly. The increasing correlation between the particular cooling (SCC) and desorption temperature is caused by growth in the latter, which promotes excellent desorption and enhances the efficiency of adsorption refrigeration.

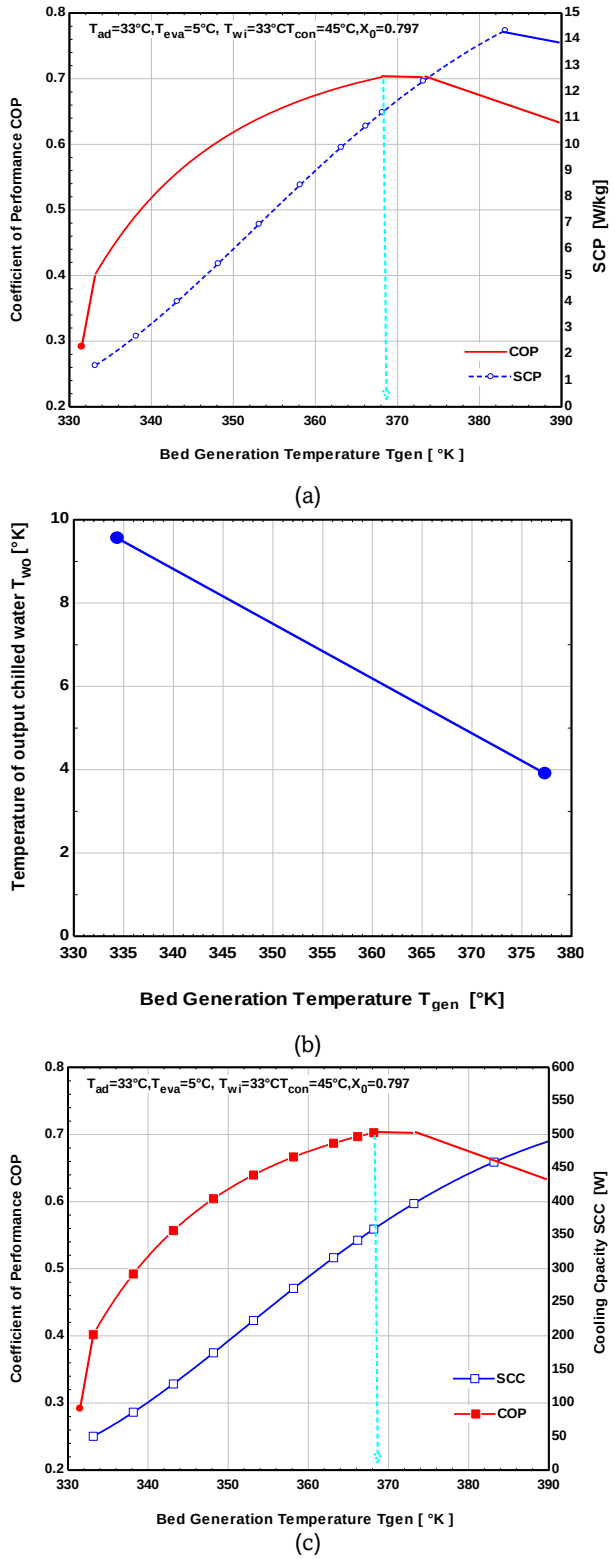


**Fig. 16.** (a).The bed generation temperature affects COP and SCP, (b) affects chilled output water temperature (Two), and (c) Hot inlet water temperature affects COP and SCC.

*5.1.12. Hot and cool inlet water temperature affects the cooling capacity and COP*

The current work aims to create a cooling system that can effectively provide cooling by combining ambient temperate coolant with low-temperature waste heat sources. Plotting the simulated results of variations in cooling capacity SCC and COP with hot water intake temperature, fixed cooling water, and chilled water inlet temperatures are shown in Fig. 17a. When the temperature of the hot water inlet is raised from (60 to 95°C), the cooling capacity increases linearly from 50.4 W to 359 W. This is because there is an increase in refrigerant circulation because of this greater driving source temperature leads to increased refrigerant desorption and increased refrigerant circulation. For hot water, temperature varies between 85 and 95°C, and simulated COP values peak. The COP reduction indicates reduced cooling capability for hot water inlets between (60 and 95 °C), and an increase in heat losses between (85 and 95 °C) due to the sorption components' frequent switching between adsorption and desorption modes. When the coolant intake temperature is 33°C and the hot water inlet temperature ranges from (80 to 95 °C), the optimum COP value is 0.702. The efficiency of the system increases with increasing hot water inlet temperature and lowering the cooling water inlet temperature.

The maximum generation cycle temperature is an important component that determines the SCC system. The impact of cooling water input temperatures on cooling capacity and COP are depicted in Fig. 17b. As the cooling water inlet temperature drops from (40 to 20 °C), the cooling capacity gradually rises. This is because each cycle involves a greater amount of Adsorbed and desorbed refrigerant due to lower adsorption temperatures. Reduced cooling water inlet temperature likewise results in higher simulated COP values. When the coolant temperature is (20 °C) and the hot generating temperature is (95°C), the COP value for the adsorption chiller is 0.702. When

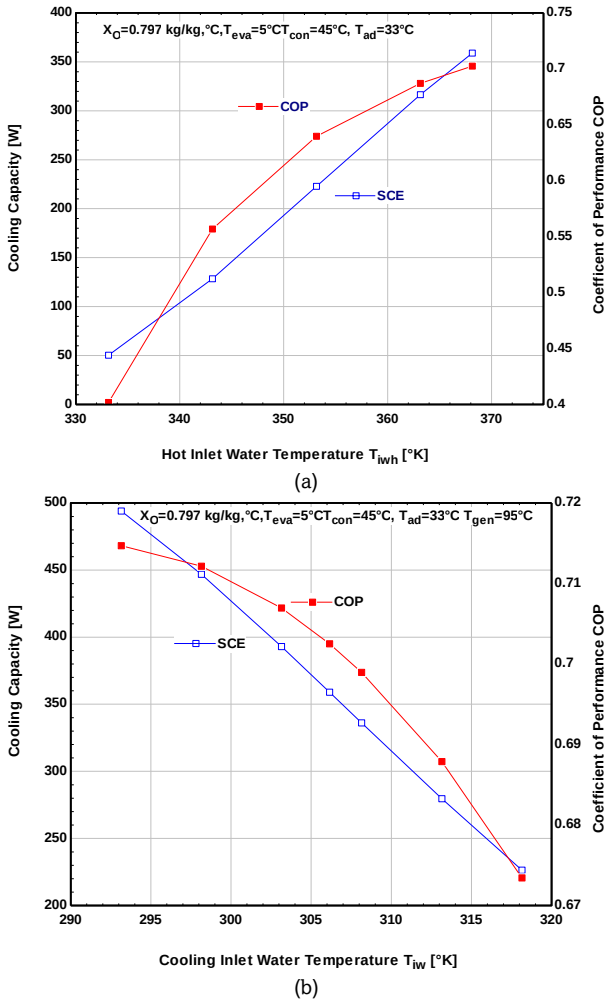


**Fig. 17.** (a). Hot inlet water temperature affects SCC and COP, (b) Effect of inlet cooling water temperature on SCC and COP

the temperature rises between evaporation-adsorption and desorption-condensation are more than 30°K, this outcome is attributable to an increase in heat losses. Those are validated with (El-Sharkawy *et al.,* 2006).

### *5.2. Comparing the current work to previous studies published in the literature*

A comparison of the performance of the current work with studies documented in the literature is presented in Table 4. The system's COP, as determined by the present mathematical simulation model, analysis, is approximately 16% greater than the value given by (Saha *et al.*, 2007). The new machine generator bed characteristics at which refrigerant adsorbs increase during the isobarically adsorbed, accelerating the desorption process and enhancing the system's refrigeration capacity. The comparison stated in Table 4, with the outcomes reported by (Faizan *et al.*, 2020), (Marzia *et al.*, 2018), and (Hadj Ammar *et al.,* 2017).

## 6. Conclusion

Under the climate conditions of Iraq, an optimization of two-bed solar adsorption cooling unit working with an activated carbon /ethanol pair is conducted. The optimal cycle performances of an adsorption system are assessed and simulated by EES with the desorption temperature range of (60 to 95 °C), evaporator temperatures of (5°C) and condensation temperature (45°C) for cooling applications. The present investigation produced the following findings. This work uses a thermodynamic analysis and a transient modeling study to describe the operating and performance characteristics of two-bed solar thermal-driven activated carbon/ethanol adsorption cooling system. According to the thermodynamic analysis, low condensation temperatures ($T_{con}$ 45°C for 80°C $\leq T_{gen} \leq$100°C) yield the best results for COP. For higher condenser temperatures, it is evident that the collector needs to be heated to a higher adsorbent temperature. However, it ought to be lower than 100°C. Converting to a total daily cooling chilled water production of 39.4 kg at approximately 5°C. At low condenser temperature ($T_{con}$ = 45 °C) and high adsorbent temperature ($T_{gen}$ 95 °C). However, at low minimum adsorbent temperatures ($T_{ad}$ < 35°C), the best outcome for freezing purposes could be obtained if the evaporator temperature is zero. As a result, the ideal pressures for the condenser and evaporator are, respectively, 23.14 kPa and 2.408 kPa., the ideal COP was 0.702 with a total energy input of 11893.5 kJ. It is well working pair for air conditioning applications but with refrigeration, COP will be less. The desorption heat is a major part of the machine heating input. According to the current analysis, it is about 69.0%. The system's maximum and minimum adsorbate concentration ratios, 0.12 kg/kg and 0.5152 kg/kg with Δx 0.39 kg/kg were recorded during this cycle. The corresponding mass of refrigerant adsorbed is estimated to be 1.92 kg and 8.24 kg, respectively. Consequently, 6.32 kg is the operative Ethanol mass cycling through this system and 76.0 % is the productivity of ethanol. There is a linear relation between SCE and bed generation temperature, due to the increase in Δx as increasing bed generation temperature. The relation between COP condensation pressure is the opposite because adsorption and desorption do not begin until the pressure in the bed generator reaches the saturation pressure, which is determined by the temperature of the evaporator and the condensation pressure, respectively. Cooling capacity and COP are increased with hot water temperature increasing and with the reduction of inlet cooling

**Table 4**
Evaluation of the present research and other studies

| Study | Working Pair | work | COP |
|---|---|---|---|
| Present study | AC/ethanol | EES Simulation | 0.702 |
| Asif Sha et al., 2021 | AC/ethanol | Matlab simulation | 0.68 |
| Shabir *et al.,* 2020 | AC/ethanol | Simulation | 0.61 |
| Khanam *et al.,* 2018 | AC/ethanol | CFD Simulation | 0.61 |
| Frazzica *et al.,* 2016 | AC/ethanol | experimentally | 0.63 |
| Saha *et al.,* 2007 | AC/ethanol | Simulation | 0.59 |
| Hadj Ammar. *et al* 2017 | AC/methanol | Simulation | 0.73 |

water temperature. The condensation temperature is inversely proportional to COP and SCP for single and double stages. For improving cop with ethanol refrigerator, can use silica gel/ethanol as a working pair, or ethanol with metal-organic frameworks (MOF) or consolidated composite adsorbents.

## Nomenclature

| Symbols | Nomenclature | Units |
|---|---|---|
| mAC | Mass of A.C | kg |
| $C_{AC}$ | The specific heat of activated carbon | (kJ.kg$^{-1}$.K$^{-1}$) |
| $c_{ice}$ | The specific heat of ice | (kJ.kg$^{-1}$.K$^{-1}$) |
| $C_{wall}$ | Specific heat of the wall (shell +tube) | (kJ.kg$^{-1}$.K$^{-1}$) |
| $C_{eth}$ | Specific heat of Ethanol | (kJ.kg$^{-1}$.K$^{-1}$) |
| $C_w$ | Specific heat of water | (kJ.kg$^{-1}$.K$^{-1}$) |
| $C_{eth}$ | Specific heat of evaporation | (kJ.kg$^{-1}$.K$^{-1}$) |
| D | the constant of Dubinin–Astakhov | K$^{-1}$ |
| n | the constant of Dubinin–Astakhov | |
| mwall | Mass, of the wall | kg |
| H | The isosteric heating of ads/des | kJ/kg |
| L | The latent heat | kJ/kg |
| Q | Sensible heat | kJ |
| $h_{fu}$ | Enthalpy fusion state | kJ/kg |
| $h_{ad}$ | The isosteric heating of ads | kJ/kg |
| $h_{fg}$ | The latent heating enthalpy of the liquid-vapor phase conversion | kJ/kg |
| $L_{ice}$ | The latent heating of fusion of ice | k/kg |
| $m_r$ | The refrigerant mass | kg |
| $m_{eth.}$ | The ethanol mass | kg |
| $m_{shell}$ | Mass of shell | kg |
| $m_{tube}$ | Mass of tubes | kg |
| $m_w$ | Mass of water | kg |
| $m_{ice}$ | Mass of ice | kg |
| $m_{cwc}$ | Mass of cooled water | kg |
| $\dot{m}$ | Mass flow rate | (kg /s) |
| $P_{con}$ | Condenser pressure | k$Pa$ |
| $P_{gen}$ | Generator pressure | k$Pa$ |
| $P_{Sat}$ | Saturation vapor pressure | k$Pa$ |
| $P_{eva}$ | evaporator pressure | k$Pa$ |
| $P$ | Pressure | k$Pa$ |
| $Q_{eva}$ | Sensible heat of the evaporator | kJ |
| $Q$ | Heat-flow | kJ |
| R | Gas constant | (kJ.kg$^{-1}$.K$^{-1}$) |
| t | Time | hr |
| $t_{cycle}$ | Cycle time | sec |
| $T$ | Temperature | ℃ |
| $T_{eva}$ | The evaporated temperature of ethanol in the evaporator | ℃ |
| $T_{gen}$ | The bed generation temperature | ℃ |
| $T_{con}$ | Condenser temperature | ℃ |
| $T_{sat}$ | Saturation temperature | ℃ |
| $T_{ambiant}$ | Ambient temperature | ℃ |
| $T_{ad}$ | The temperature of adsorption | ℃ |
| $T_{sd}$ | The starting temperature of desorption | ℃ |
| $T_{sa}$ | The starting temperature of adsorption | ℃ |
| $T_{wi}$ | The initial temperature of the water | ℃ |
| $U$ | Internal energy | kJ |
| $x_0 = X_0$ | The maximum-adsorption uptake | kg/kg |
| $x = X$ | The equilibrium adsorbate-concentration ratio | kg/kg |
| Imax | The maximum solar radiation | W/m$^2$ |

**Abbreviation**

| | | |
|---|---|---|
| COP | Coefficient of performance | |
| EES | Engineering equation solver software | |
| SCC | Cooling capacity | W |
| SCE | Specific-cooling effect | kJ/kg |
| SCP | Specific-cooling power | W/Kg |
| V | Valve | |

**Greek letter**

| | | |
|---|---|---|
| $\gamma$ | The total adsorption bed porosity | – |
| Δ | Change /difference | – |
| $\rho$ | Density | $(kg/m^3)$ |
| $\boldsymbol{\rho_{sat}}$ | Saturation Density | $(kg/m^3)$ |
| $\theta$ | Adsorbate Volume Fraction | |
| μ | Dryness factor of adsorbate | |

**Subscripts**

| | |
|---|---|
| *A.C* | Activated carbon |
| *ad* | Adsorption |
| *des* | Desorption quantity |
| *C.V.* | Control volume |
| *f* | Fluid |
| *e* | Exit state |
| *g* | Gas |
| *l* | Liquid |
| *eth* | Ethanol |
| *r* | Refrigerant |
| *f* | The liquid phase of the refrigerant |
| *max* | Maximum |
| *min* | Minimum |
| *gen* | Generation |
| *con* | Condensation |
| *sat* | Saturation |
| *v* | The volume filed with the adsorbed phase |
| *eva* | Evaporation |

## Acknowledgments

I would like to give special thanks to my family as a whole for their continuous support and understanding when undertaking my research and writing my project. Your prayer for me was what sustained me this far.

**Funding:** This research does not receive financial support.

**Conflicts of Interest:** The author declares there are no conflicts of interest.

## References

Abass, A. Z., & Pavlyuchenko, D. (2019). Turning Iraq into a Country of Energy Exporters through the Exploitation of Solar Energy and West Desert Land. *E3S Web of Conferences*, 114, 05009. https://doi.org/10.1051/e3sconf/201911405009

Abdulkadir, M., Kulla, D., & Pam, G. (2022, August 24). Performance Evaluation of Date-Seed Activated Carbon as Adsorbent in Adsorption Refrigeration System. *Nigerian Journal of Basic and Applied Sciences,* 30(1), 24–27. https://doi.org/10.4314/njbas.v30i1.3

Ahmed, B. M., & Alhialy, N. F. F. (2020, March 31). Experimental and Theoretical Analysis of a Mono PV Cell with Five Parameters, Simulation Model Compatible with Iraqi Climate. *Association of Arab Universities Journal of Engineering Sciences*, 27(1), 54–64. https://doi.org/10.33261/jaaru.2019.27.1.007

Ahmed, B. M., & Farman Alhialy, N. F. (2019, August 25). Optimum Efficiency of PV Panel Using Genetic Algorithms to Touch Proximate Zero Energy House (NZEH). *Civil Engineering Journal,* 5(8), 1832–1840. https://doi.org/10.28991/cej-2019-03091375

Alamoudi, H. A., & Abdel-Dayem, A. M. (2021, October 27). Design Optimization and Simulation of an Ice Plant Working By Solar Adsorption Technology. *European Journal of Energy Research*, 1(4), 13–22. https://doi.org/10.24018/ejenergy.2021.1.4.22

Asif Sha, A., Baiju, V., Rehna, R., Suzuki, T., Singh, H., & Ichiyanagi, M. (2022, November). Performance Investigations of Carbon Based Consolidated Composite Adsorbents Effective for Adsorption Cooling Systems. *Applied Thermal Engineering*, 217, 119199. https://doi.org/10.1016/j.applthermaleng.2022.119199

Boruta, P., Bujok, T., Mika, U., & Sztekler, K. (2021, August 3). Adsorbents, Working Pairs, and Coated Beds for Natural Refrigerants in Adsorption Chillers—State of the Art. *Energies*, 14(15), 4707. https://doi.org/10.3390/en14154707

Bouzid, M., Bouaziz, N., Torkia, Y. B., & Lamine, A. B. (2019, June). Statistical Physics Modeling of Ethanol Adsorption onto the Phenol Resin Based Adsorbents: Stereographic, Energetic and

Thermodynamic Investigations. *Journal of Molecular Liquids*, 283, 674–687. https://doi.org/10.1016/j.molliq.2019.03.129

Bouzid, M., Sellaoui, L., Khalfaoui, M., Belmabrouk, H., & Lamine, A. B. (2016, February). Adsorption of Ethanol onto Activated Carbon: Modeling and Consequent Interpretations Based On Statistical Physics Treatment. *Physica A: Statistical Mechanics and Its Applications,* 444, 853–869. https://doi.org/10.1016/j.physa.2015.09.097

Brancato, V., Frazzica, A., Sapienza, A., Gordeeva, L., & Freni, A. (2015, May). Ethanol adsorption onto carbonaceous and composite adsorbents for adsorptive cooling system. *Energy*, *84*, 177–185. https://doi.org/10.1016/j.energy.2015.02.077

Brancato, V., Gordeeva, L., Sapienza, A., Freni, A., & Frazzica, A. (2016, July). Dynamics Study of Ethanol Adsorption on Microporous Activated Carbon for Adsorptive Cooling Applications. *Applied Thermal Engineering,* 105, 28–38. https://doi.org/10.1016/j.applthermaleng.2016.05.148

Burchell, T. (1999, July 22). Carbon Materials for Advanced Technologies. Elsevier.

Chauhan, P., Baiju, V., Asif Sha, A., & Tyagi, S. (2024, February). Adsorption of Ethanol onto Novel and Indigenous Green Adsorbents: Synthesis, Characterization, and Applications. *Journal of Cleaner Production*, 442, 140978. https://doi.org/10.1016/j.jclepro.2024.140978

Chen, Z., Wang, X., Islamoglu, T., & Farha, O. K. (2019, April 26). Green Synthesis of a Functionalized Zirconium-Based Metal–Organic Framework for Water and Ethanol Adsorption. *Inorganics*, 7(5), 56. https://doi.org/10.3390/inorganics7050056

Dakkama, H., Elsayed, A., Al-Dadah, R., Mahmoud, S., & Youssef, P. (2015). Investigation of Cascading Adsorption Refrigeration System with Integrated Evaporator-Condenser Heat Exchanger Using Different Working Pairs. *Energy Procedia*, 75, 1496–1501. https://doi.org/10.1016/j.egypro.2015.07.285

Denzinger, C., Berkemeier, G., Winter, O., Worsham, M., Labrador, C., Willard, K., Altaher, A., Schuleter, J., Ciric, A., & Choi, J. K. (2021, January). Toward Sustainable Refrigeration Systems: Life Cycle Assessment of a Bench-Scale Solar-Thermal Adsorption Refrigerator. *International Journal of Refrigeration*, 121, 105–113. https://doi.org/10.1016/j.ijrefrig.2020.09.022

El-Sharkawy, I. I., Uddin, K., Miyazaki, T., Baran Saha, B., Koyama, S., Kil, H. S., Yoon, S. H., & Miyawaki, J. (2015, February). Adsorption of Ethanol onto Phenol Resin Based Adsorbents for Developing Next Generation Cooling Systems. *International Journal of Heat and Mass Transfer*, 81, 171–178. https://doi.org/10.1016/j.ijheatmasstransfer.2014.10.012

El-Sharkawy, I. I., Uddin, K., Miyazaki, T., Saha, B. B., Koyama, S., Miyawaki, J., & Yoon, S. H. (2014). Adsorption of Ethanol onto Parent and Surface Treated Activated Carbon Powders. *International Journal of Heat and Mass Transfer*, 73, 445–455. https://doi.org/10.1016/j.ijheatmasstransfer.2014.02.046

El-Sharkawy, I., Kuwahara, K., Saha, B., Koyama, S., & Ng, K. (2006, June). Experimental Investigation of Activated Carbon Fibers/Ethanol Pairs for Adsorption Cooling System Application. *Applied Thermal Engineering*, 26(8–9), 859–865. https://doi.org/10.1016/j.applthermaleng.2005.10.010

El-Sharkawy, I., Saha, B., Koyama, S., He, J., Ng, K., & Yap, C. (2008, December). Experimental Investigation on Activated Carbon–Ethanol Pair for Solar Powered Adsorption Cooling Applications. *International Journal of Refrigeration*, 31(8), 1407–1413. https://doi.org/10.1016/j.ijrefrig.2008.03.012

Elsheniti, M. B., Elsamni, O. A., Al-Dadah, R. K., Mahmoud, S., Elsayed, E., & Saleh, K. (2018, June 13). Adsorption Refrigeration Technologies. Sustainable Air Conditioning Systems. https://doi.org/10.5772/intechopen.73167

Farman, N. F., Redha, Z. A. A., & Mahdi, S. A. (2017, December). Optimization of the Efficiency of Continuous Solar Adsorption Refrigeration System with Genetic Algorithm. *2017 2nd International Conference on the Applications of Information Technology in Developing Renewable Energy Processes & Systems (IT-DREPS)*. https://doi.org/10.1109/it-dreps.2017.8277821

Frazzica, A., Palomba, V., Dawoud, B., Gullì, G., Brancato, V., Sapienza, A., Vasta, S., Freni, A., Costa, F., & Restuccia, G. (2016, July). Design, Realization, and Testing of an Adsorption Refrigerator Based on Activated Carbon/Ethanol Working Pair. *Applied Energy,* 174, 15–24. https://doi.org/10.1016/j.apenergy.2016.04.080

Gautam, Chaudhary, A., Singh, A., Singh, P. K., & Sahoo, S. (2024, January 24). Experimental Investigation and Thermodynamic Analysis of Coconut-Shell-Derived Activated Carbon for $CO_2$-Based Advanced Adsorption Cooling Systems. *Industrial & Engineering Chemistry Research,* 63(5), 2395–2415. https://doi.org/10.1021/acs.iecr.3c03789

H Al-Maamory, N., & Fadel Farman, N. (2023, July 1). Performance of Solar Adsorption Cooling System Using Methanol and Activated Carbon as a Working Pair. *Journal of Engineering*, 29(7), 71–85. https://doi.org/10.31026/j.eng.2023.07.05

Hadj Ammar, M., Benhaoua, B., & Bouras, F. (2017, February). Thermodynamic Analysis and Performance of an Adsorption Refrigeration System Driven By Solar Collector. *Applied Thermal Engineering,* 112, 1289–1296. https://doi.org/10.1016/j.applthermaleng.2016.09.119

Hasan Rupam, T., Ahmed Rocky, K., Palash, M. L., & Baran Saha, B. (2023, January). Ethanol Adsorption onto Various Metal-Organic Frameworks for Cooling Applications. *Thermal Science and Engineering Progress,* 37, 101602. https://doi.org/10.1016/j.tsep.2022.101602

Kalawa, W., Sztekler, K., Mlonka-Mędrala, A., Radomska, E., Nowak, W., Mika, U., Bujok, T., & Boruta, P. (2023, August 5). Simulation Analysis of Mechanical Fluidized Bed in Adsorption Chillers. *Energies*, 16(15), 5817. https://doi.org/10.3390/en16155817

Khanam, M., Jribi, S., Miyazaki, T., Saha, B., & Koyama, S. (2018, June 8). Numerical Investigation of Small-Scale Adsorption Cooling System Performance Employing Activated Carbon-Ethanol Pair. *Energies*, 11(6), 1499. https://doi.org/10.3390/en11061499

Lache, M., Kappelhoff, C., Seiler, J., & Bardow, A. (2023, January 18). Water and Ethanol as Refrigerant Mixture Enabling Adsorption Cooling Below 0 °C. *Energy Technology*, 11(3). https://doi.org/10.1002/ente.202201158

Li, M., Huang, H., Wang, R., Wang, L., Cai, W., & Yang, W. (2004, December). Experimental Study on Adsorbent of Activated Carbon with Refrigerant of Methanol and Ethanol for Solar Ice Maker. *Renewable Energy*, 29(15), 2235–2244. https://doi.org/10.1016/j.renene.2004.04.006

Miyazaki, T., El-Sharkawy, I I., Saha, B., and Koyama, S, (2014). Optimized Performance of one-Bed Adsorption Cooling System. *International Refrigeration and Air Conditioning Conference. Paper 1480*. http://docs.lib.purdue.edu/iracc/1480

Mustafa, R., Mohd Radzi, M. A. B., Hizam, H. B., & Che Soh, A. (2024). An innovative air-cooling system for efficiency improvement of retrofitted rooftop photovoltaic module using cross-flow fan. *International Journal of Renewable Energy Development*, 13(2), 223-234. https://doi.org/10.61435/ijred.2024.60068

Pal, A., El-Sharkawy, I. I., Saha, B. B., Jribi, S., Miyazaki, T., & Koyama, S. (2016, October). Experimental Investigation of $CO_2$ Adsorption onto a Carbon-Based Consolidated Composite Adsorbent for Adsorption Cooling Application. *Applied Thermal Engineering*, 109, 304–311. https://doi.org/10.1016/j.applthermaleng.2016.08.031

Patel, J., & Maiti, S. (2023). Experimental Investigation of a Small-Scale Evacuated Tube-Based Solar Adsorption Chiller with Emphasis on Improving the Cycle Time. *Energy Conversion and Management,* 292, 117421. https://doi.org/10.1016/j.enconman.2023.117421

Patrick & Khalidah. (n.d.). Iraq Has an Opportunity to Become a Solar Leader. (2010)

Qasem, N. A., & El-Shaarawi, M. A. (2015, August). Thermal Analysis and Modelling Study of an Activated Carbon Solar Adsorption Icemaker: Dhahran case study. *Energy Conversion and Management,* 100, 310–323. https://doi.org/10.1016/j.enconman.2015.04.054

Rezk, A., Gediz Ilis, G., & Demir, H. (2022, September). Experimental Study on Silica Gel/Ethanol Adsorption Characteristics for Low-Grade Thermal Driven Adsorption Refrigeration Systems. *Thermal Science and Engineering Progress*, 34, 101429. https://doi.org/10.1016/j.tsep.2022.101429

Rupa, M. J., Pal, A., & Saha, B. B. (2020, February). Activated Carbon-Graphene Nanoplatelets Based Green-Cooling System: Adsorption Kinetics, Heat of Adsorption, And Thermodynamic Performance. *Energy,* 193, 116774. https://doi.org/10.1016/j.energy.2019.116774

Saadoon, T. N., Farman, N. F., & Mustafa, F. I. (2020, October 29). Thermal Efficiency Optimization of the Evacuated Tube Solar Water Heater System by Using Mirror Flat Reflector. 2020 11th *International Renewable Energy Congress (IREC)*. https://doi.org/10.1109/irec48820.2020.9310380

Saha, B., El-Sharkawy, I., Chakraborty, A., Koyama, S., & Ng, K. C. (2006). Study on Acf/Ethanol Based Two-Stage Adsorption Cooling Cycle. *Multiphase*. https://doi.org/10.1615/ihtc13.p12.470

Saha, B. B., El-Sharkawy, I. I., Shahzad, M. W., Thu, K., Ang, L., & Ng, K. C. (2016, March). Fundamental And Application Aspects Of Adsorption Cooling And Desalination. *Applied Thermal Engineering,* 97, 68–76. https://doi.org/10.1016/j.applthermaleng.2015.09.113

Saha, B., El-Sharkawy, I., Chakraborty, A., & Koyama, S. (2007, January). Study on an Activated Carbon Fiber–Ethanol Adsorption Chiller: Part I – System Description And Modelling. *International Journal of Refrigeration,* 30(1), 86–95. https://doi.org/10.1016/j.ijrefrig.2006.08.004

Saha, B., El-Sharkawy, I., Chakraborty, A., & Koyama, S. (2007, January). Study an Activated Carbon Fiber–Ethanol Adsorption Chiller: Part II – Performance Evaluation. *International Journal of Refrigeration,* 30(1), 96–102. https://doi.org/10.1016/j.ijrefrig.2006.08.005

Sghaier, W., Ben Torkia, Y., Bouzid, M., & Ben Lamine, A. (2022, September). Thermodynamic Analysis Of Cooling Cycles Based on Statistical Physics Modeling Of Ethanol Adsorption Isotherms. *International Journal of Refrigeration*, 141, 119–131. https://doi.org/10.1016/j.ijrefrig.2022.05.022

Sha, A. A., & Baiju, V. (2021, March). Thermodynamic Analysis and Performance Evaluation of Activated Carbon-Ethanol Two-Bed Solar Adsorption Cooling System. *International Journal of Refrigeration,* 123, 81–90. https://doi.org/10.1016/j.ijrefrig.2020.12.006

Shabir, F., Sultan, M., Niaz, Y., Usman, M., Ibrahim, S. M., Feng, Y., Naik, B. K., Nasir, A., & Ali, I. (2020, August 28). Steady-State Investigation of Carbon-Based Adsorbent–Adsorbate Pairs for Heat Transformation Application. *Sustainability*, 12(17), 7040. https://doi.org/10.3390/su12177040

Sowunmi, A. R., Folayan, C. O., Anafi, F. O., Ajayi, O., Omisanya, N. O., Edet, A. A., Oyedeji, A. N., & Salami, K. A. (2023, March 31). Simulation of the Performance of Continuous Solar-Powered Adsorption Refrigeration System for Optimal Use in Zaria, Nigeria. *Proceedings of the Institution of Mechanical Engineers, Part C: Journal of Mechanical Engineering Science*. https://doi.org/10.1177/09544062231163427

Tarish, A. L., Khalifa, A. H. N., & Hamad, A. J. (2020, November 1). Methods of Improving the Performance of Adsorption Thermophysical Battery Based on the Operating Conditions and Structure: A Review. *IOP Conference Series: Materials Science and Engineering*, 928(2), 022040. https://doi.org/10.1088/1757-899x/928/2/022040

Tiansuwan and Hirunlabh, J. (1998). Mathematical Model of an Activated Carbon-Ethanol Refrigerator. *Thammasat Int.J.Sc.Tec*, (1998). 3(1).

Uddin, K., El-Sharkawy, I. I., Miyazaki, T., Saha, B. B., & Koyama, S. (2014, March). Thermodynamic Analysis of Adsorption Cooling Cycle Using Ethanol-Surface Treated Maxsorb III Pairs. *Evergreen*, 1(1), 25–31. https://doi.org/10.5109/1440973

Uddin, K., El-Sharkawy, I.I., Miyazaki, T., Saha, B., & Koyama, S. (2014). Thermodynamic Analysis of Adsorption Refrigeration Cycles Using Parent and Surface Treated Maxsorb III/Ethanol Pairs. *International Refrigeration and Air Conditioning Conference*. Paper 1493. https://docs.lib.purdue.edu/iracc/1493/

Uddin, K., Miyazaki, T., Koyama, S., & Saha, B. B. (2013, December). Performance Investigation of Adsorption–Compression Hybrid Refrigeration Systems. *International Journal of Air-Conditioning and Refrigeration,* 21(04), 1350024. https://Doi.org/10.1142/S2010132513500247

Umair, M., Akisawa, A., & Ueda, Y. (2014, March 11). Performance Evaluation of a Solar Adsorption Refrigeration System with a Wing Type Compound Parabolic Concentrator. *Energies,* 7(3), 1448–1466. https://doi.org/10.3390/en7031448

© 2024. The Author(s). This article is an open-access article distributed under the terms and conditions of the Creative Commons Attribution-ShareAlike 4.0 (CC BY-SA) International License (http://creativecommons.org/licenses/by-sa/4.0/)